# EXCITATION OF NII LINES FROM DISSOCIATION OF
# $N_2$ AND NO BY ELECTRON COLLISION

VON KÁRMÁN GAS DYNAMICS FACILITY
ARNOLD ENGINEERING DEVELOPMENT CENTER
AIR FORCE SYSTEMS COMMAND
ARNOLD AIR FORCE STATION, TENNESSEE 37389

PROPERTY OF U.S. AIR
AEDC TECHNICAL LIBRARY

July 1975

Final Report for Period May 1, 1973 — November 1, 1974

TECHNICAL REPORT
FILE COPY

Approved for public release; distribution unlimited.

Prepared for

DIRECTORATE OF TECHNOLOGY
ARNOLD ENGINEERING DEVELOPMENT CENTER
ARNOLD AIR FORCE STATION, TENNESSEE 37389

This report has been reviewed by the Information Office (OI) and is releasable to the National Technical Information Service (NTIS). At NTIS, it will be available to the general public, including foreign nations.

## APPROVAL STATEMENT

This technical report has been reviewed and is approved for publication.

FOR THE COMMANDER

KENNETH B. HARWOOD
Captain, CF
Research & Development
   Division
Directorate of Technology

ROBERT O. DIETZ
Director of Technology

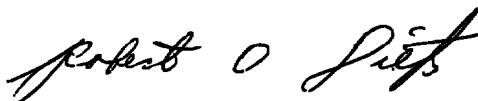| REPORT DOCUMENTATION PAGE | | READ INSTRUCTIONS BEFORE COMPLETING FORM |
|---|---|---|
| 1 REPORT NUMBER<br>AEDC-TR-75-77 | 2 GOVT ACCESSION NO. | 3. RECIPIENT'S CATALOG NUMBER |
| 4 TITLE (and Subtitle)<br>EXCITATION OF NII LINES FROM DISSOCIATION OF $N_2$ AND NO BY ELECTRON COLLISION | | 5 TYPE OF REPORT & PERIOD COVERED<br>Final Report - May 1, 1973 - November 1, 1974 |
| | | 6 PERFORMING ORG. REPORT NUMBER |
| 7. AUTHOR(s)<br>J. R. Gilbert and J. W. L. Lewis<br>ARO, Inc. | | 8 CONTRACT OR GRANT NUMBER(s) |
| 9 PERFORMING ORGANIZATION NAME AND ADDRESS<br>Arnold Engineering Development Center (XO)<br>Arnold Air Force Station (DY)<br>Tennessee 37389 | | 10 PROGRAM ELEMENT, PROJECT, TASK AREA & WORK UNIT NUMBERS<br>Program Element 65807F |
| 11. CONTROLLING OFFICE NAME AND ADDRESS<br>Arnold Engineering Development Center (DYFS), Arnold Air Force Station, Tennessee 37389 | | 12. REPORT DATE<br>July 1975 |
| | | 13. NUMBER OF PAGES<br>65 |
| 14 MONITORING AGENCY NAME & ADDRESS(If different from Controlling Office) | | 15 SECURITY CLASS. (of this report)<br>UNCLASSIFIED |
| | | 15a. DECLASSIFICATION/DOWNGRADING SCHEDULE<br>N/A |

16 DISTRIBUTION STATEMENT (of this Report)

Approved for public release; distribution unlimited.

17. DISTRIBUTION STATEMENT (of the abstract entered in Block 20, If different from Report)

18 SUPPLEMENTARY NOTES

Available in DDC

19 KEY WORDS (Continue on reverse side if necessary and identify by block number)

| | | |
|---|---|---|
| optical measurements | fluorescence | electron scattering |
| collision cross sections | nitrogen | electron beams |
| mathematical analysis | density | radiative transitions |

20 ABSTRACT (Continue on reverse side If necessary and identify by block number)

The ionized atomic nitrogen NII lines at 3995.0 and 5016.4 Å were produced by dissociative excitation of gaseous $N_2$ and NO by electron beam impact. The dependence of the optical radiative intensity on electron beam energy over the range of 4 to 20 keV was used to determine the relative optical dissociative excitation cross sections of these two radiating NII levels. The relative cross sections were normalized to the known cross-section value of

DD $_{1 \text{ JAN } 73}^{\text{FORM}}$ 1473   EDITION OF 1 NOV 65 IS OBSOLETE

20. ABSTRACT (Continued)

the (0,0) band of the $N_2^+$ First Negative System, and the results are analyzed using the Bethe-Born approximation.

# PREFACE

The work reported herein was conducted by the Arnold Engineering Development Center (AEDC), Air Force Systems Command (AFSC), Arnold Air Force Station, Tennessee, under Program Element 65807F. The results were obtained by ARO, Inc. (a subsidiary of Sverdrup & Parcel and Associates, Inc.), contract operator of AEDC, AFSC. The work was conducted under ARO Project No. V32S-46A(VF420). The authors of this report were J. R. Gilbert and J. W. L. Lewis, ARO, Inc. The manuscript (ARO Control No. ARO-VKF-TR-75-3) was submitted for publication on January 15, 1975.

# CONTENTS

# ILLUSTRATIONS

## TABLES

# 1.0 INTRODUCTION

## 1.1 BACKGROUND

The excitation of gaseous atomic and molecular species by high-energy electron impact has long been of fundamental interest. However, during recent years additional attention has been given this subject because of the applications of such knowledge including the use of electron impact excitation for determining various properties of the gaseous species. Our own interest is motivated by the use of electron beam fluorescence diagnostics of high-speed flow fields of gases and their mixtures for the purpose of determining local values of gas specie density and temperature by observing the fluorescence radiation resulting from electron-molecule collisions of 5 to 50 keV energy. Although the breadth of the energy range of interest is somewhat arbitrary, various application restraints do exist that place practical limits on both the lower and upper bound of the electron energy. The primary constraint encountered in diagnostic applications is that of an electron beam spreading along the injection path as a result of both elastic and inelastic scattering processes, thereby degrading the spatial resolution. Consequently, on this basis, one would desire to employ beam energies on the order of 50 keV to minimize spreading problems; energies greater than about 50 keV are obviously practical, but little is gained in the area of beam spreading by so doing, and such high energies are not deemed worth the added arcing and corona discharge problems encountered.

A second, but less important, consideration is encountered when applying this technique to the measurement of low gas density samples as are typically found in the far field of hypersonic expansions. For these cases, one desires as much radiative intensity as is possible within the spatial resolution requirements, and consequently, the use of lower beam energies and, thereby, larger cross sections is attractive. A lower limit of 1 to 5 keV for electron beam energy in these instances is not unreasonable.

As will be discussed in detail in a following section, the electron-molecule excitation process can be categorized according to the changes in angular momentum and spin quantum numbers resulting from the collision. Generally, such collisions are denoted as allowed or forbidden, and the degree of forbiddenness can be further refined as forbidden in orbital angular momentum or spin angular momentum or both, and each type of transition is experimentally characterized by its

dependence on electron energy. As is well known, in general, the allowed transitions are much stronger than those which are first-order forbidden, and as a result, allowed transitions are usually employed for diagnostics applications. However, even though allowed transitions are preferable for use, one cannot ignore the weaker, forbidden transitions for many applications. As an example, if one is studying the flow field of a binary mixture of He and $N_2$ for which the He mole fraction is small, the strong, allowed He transition $3^1P \rightarrow 2^1S$ at 5016 Å can easily be obscured by the NII transition $3F° \rightarrow 3D$ at 5016.4 Å, which is the result of the dissociative-excitation of $N_2$ by electron impact. Obviously, both for experiment design as well as data interpretation the dependence of the NII line excitation cross section with electron energy as well as its absolute value, density and current dependences are desired. A related question exists when one considers flow fields containing the molecule and at least one of its constituent atomic species, such as $N_2/N$, NO/N or O, $H_2/H$, HF/H or F, and $F_2/F$ mixtures. Obviously, to determine the density of the atomic specie, say N, radiative transitions of the NI or NII species must be observed; higher ionized species such as NIII, NIV, etc., are quite unlikely. Since the electron impact on both N as well as $N_2$ produces NI and NII radiation, one desires to know to what extent the molecular and atomic species each contribute to the resulting composite radiation. To do so, one must know the cross section for the production of each specie as well as its energy dependence. For the atomic specie, inspection and comparison of the ground state quantum number description with that of the excited, radiating state can, in many cases, give one the gross characterization of the excitation process as either allowed or forbidden. The situation is less simple for dissociation processes for molecules, since the process involved is at least three-body in nature.

This report, which is the first in a series of studies of dissociative-excitation processes of electron-molecule collisions, describes the results of the measurement of the energy dependence of the dissociative-ionization cross sections for the excitation of the NII states $3F°$ and $1D$ by electron impact on both $N_2$ and NO. The results were anticipated to characterize each transition as to whether it is allowed or forbidden and to determine the degree of linearity of the radiative intensity with gas density and electron beam current. Finally, the study was expected to show to what extent, if any, the excitation cross sections were affected by chemical binding. As the following sections show, these goals were achieved.

## 1.2 THEORY

The three types of electron excitation processes of interest for this work are as follows:

Molecular ionization,

$$e^- + N_2 \rightarrow (N_2^+)^* + 2e^-$$
$$\qquad\qquad \hookrightarrow N_2^+ + h\nu \qquad\qquad (1)$$
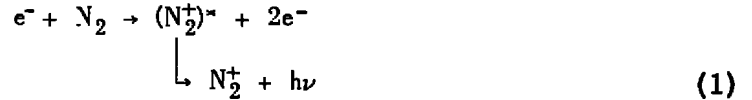
Homonuclear molecular dissociative ionization,

$$e^- + N_2 \rightarrow (N^+)^{**} + N + 2e^-$$
$$\qquad\qquad \hookrightarrow (N^+)^* + h\nu \qquad\qquad (2)$$
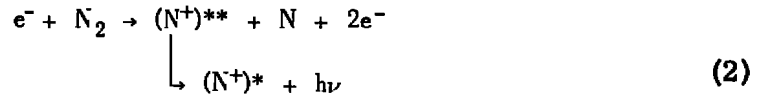
Heteronuclear molecular dissociative ionization

$$e^- + NO \rightarrow (N^+)^{**} + O + 2e^-$$
$$\qquad\qquad \hookrightarrow (N^+)^* + h\nu \qquad\qquad (3)$$
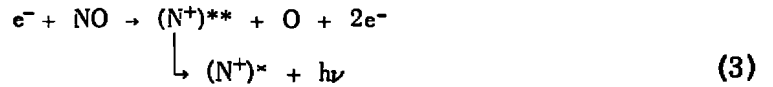
where $(\ )^*$ denotes an excited state of the parenthetically designated specie.

For the processes represented by Eqs. (1) to (3), it is assumed and the experiment is configured such that no collisional quenching effects exist.

The radiative transitions of interest are

$$N_2^- \ B^2\Sigma_u^+ \rightarrow N_2^+ \ X^2\Sigma_g^+$$
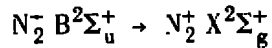
for the process of Eq. (1) and

$$NII\,^1D \rightarrow NII\,^1P^\circ$$

and

$$NII\,^3F^\circ \rightarrow NII\,^3D$$

9
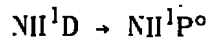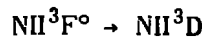
for the processes of Eqs. (2) and (3). The following paragraphs in this section describe the theoretical basis for the description of electron/atom-molecule collisions, and the section concludes with the application of the theory to the processes of Eqs. (1), (2), and (3).

## 1.2.1 Differential Cross Section

The present derivation and discussion essentially follows that of Inokuti (Ref. 1). Consider an electron of velocity $\vec{v}$ which collides with a stationary atom in its ground state and is inelastically scattered in the spherical polar direction $(\theta, \phi)$ of the center of mass system into the solid angle element $(d\omega)$, and assume that the atom undergoes a transition from the ground state (o) to state (n) of excitation energy $(E_n)$.

When the incident electron is sufficiently fast, the collision may be regarded as a sudden and small external perturbation on the target atom. The differential cross section $(d\sigma_n)$, calculated in the first Born approximation, is then given by (Ref. 1):

$$d\sigma_n = (\widetilde{M}^2/4\pi^2\hbar^4)(k'/k) \left| \int \exp(i\vec{K} \cdot \vec{r}) \psi_n^*(\vec{r}_1 \ldots \vec{r}_Z) V \psi_o(\vec{r}_1 \ldots \vec{r}_Z) d^Z\vec{r} \, d\vec{r} \right|^2 d\omega \quad (4)$$

where $\widetilde{M}$ is the reduced mass, $\vec{r}$ is the position of the incident electron relative to the center of the atom, $\hbar\vec{k}$ and $\hbar\vec{k}'$ are the initial and final momenta of the incident electron, $\hbar\vec{K} = \hbar(\vec{k} - \vec{k}')$ is the momentum transfer, and the $\psi$'s are the atomic eigenfunctions as functions of the coordinates $\vec{r}_j$ of the atomic electrons. The 3Z-dimensional volume element is denoted as

$$d^Z\vec{r} = d\vec{r}_1 \, d\vec{r}_2 \, d\vec{r}_3 \cdots d\vec{r}_Z$$

The interaction energy V is the Coulomb interaction between the incident and atomic electrons,

$$V = -\sum_{j=1}^{Z} e^2 \left| \vec{r} - \vec{r}_j \right|^{-1} \quad (5)$$

The nuclear interaction energy has been omitted in Eq. (5) since it yields no contribution to Eq. (4) due to the orthogonality of initial and final states.

By using the Bethe relation,

$$\int \exp\left(i\vec{K} \cdot \vec{r}\right)\left|\vec{r} - \vec{r}_j\right|^{-1} d\vec{r} = 4\pi K^{-2} \exp\left(i\vec{K} \cdot \vec{r}_j\right) \tag{6}$$

Eq. (4) becomes

$$d\sigma_n = \left(4\widetilde{M}^2 e^4 / \hbar^4 K^4\right)\left(k'/k\right)\left|\epsilon_n(\vec{K})\right|^2 d\omega \tag{7}$$

where $\epsilon_n(\vec{K})$ is the atomic matrix element

$$\epsilon_n(\vec{K}) = \left\langle n \left| \sum_{j=1}^{Z} \exp\left(i\vec{K} \cdot \vec{r}_j\right) \right| 0 \right\rangle = \int \psi_n^* \sum_{j=1}^{Z} \exp\left(i\vec{K} \cdot \vec{r}_j\right)\psi_o \, d^Z\vec{r} \tag{8}$$

Generally, one may consider $d\sigma_n$ as independent of $\phi$ because the ground state is spatially symmetric or because the atoms are oriented at random and an average of all atomic orientations is implied. Thus, $\left|\epsilon_n(\vec{K})\right|^2$ is a function of a scalar variable K, and one writes $\left|\epsilon_n(K)\right|^2$ instead of $\left|\epsilon_n(\vec{K})\right|^2$. Further, when one expresses $d\sigma_n$ in terms of dK, one implies integration over $\phi$ since K is independent of $\phi$. Therefore, one replaces $d\omega$ by $2\pi \sin\theta d\theta = \pi(kk')^{-1} d(K^2)$ in Eq. (7) to obtain

$$d\sigma_n = \left(4\pi \widetilde{M}^2 e^4 / \hbar^4 K^4 k^2\right)\left|\epsilon_n(K)\right|^2 d(K^2) \tag{9}$$

The quantity $\epsilon_n(K)$ reflects the dynamics of the atom and is known as the inelastic-scattering form factor. For our purposes, however, one more often uses the generalized oscillator strength:

$$f_n(K) = \left(2mE_n / \hbar^2 K^2\right)\left|\epsilon_n(K)\right|^2 \tag{10}$$

where m is the electron mass. By using the Bohr radius $a_o = \hbar^2/mc^2 = 0.52918 \times 10^{-8}$ cm and the Rydberg energy $R = me^4/2\hbar^2 = 13.606$ eV, Eq. (10) becomes

$$f_n(k) = \left(E_n/R\right)\left(Ka_o\right)^{-2}\left|\epsilon_n(K)\right|^2 \tag{11}$$

The generalized oscillator strength is a straightforward generalization of the optical (dipole) oscillator strength $f_n$, defined as

$$f_n = \left(E_n/R\right)M_n^2 \tag{12}$$

where

$$M_n^2 = \left| \int \psi_n^* \sum_{j=1}^{Z} x_j \psi_o \, d^{Z} \vec{r} \right|^2 \Big/ a_o \tag{13}$$

is the dipole-matrix-element squared and $x_j$ is a component of $\vec{r}_j$. The relationship between the dipole-matrix elements and types of transitions is discussed at the end of this section. By expanding the exponential of Eq. (8) into the familiar power series and using the orthogonality of the initial and final atomic eigenstates, it can be shown that

$$\lim_{K \to o} f_n(K) = f_n \tag{14}$$

Equation (14) is especially important because it relates the collision of fast charged particles with photoabsorption processes.

When the incident particle is an electron, $mv^2/2 = E$ represents the kinetic energy, and Eq. (9) becomes

$$d\sigma_n = \frac{4\pi a_o^2}{E \cdot R} \frac{f_n(K)}{E_n \cdot R} \, d[\ell n(Ka_o)^2] \tag{15}$$

Noting that $M/m = 1$ applies approximately for incident electrons, and using the energy conservation relation,

$$(\hbar k)^2 = (\hbar k')^2 + 2\tilde{M}E_n \tag{16}$$

and the definition of $\vec{K} = \vec{k} - \vec{k}'$, we find that

$$(Ka_o)^2 = 2\left(\frac{E}{R}\right)\left\{ 1 - \frac{1}{2}\left(\frac{E_n}{E}\right) - \left[ 1 - \left(\frac{E_n}{E}\right) \right]^{\frac{1}{2}} \cos\theta \right\} \tag{17}$$

For a given value of $E_n$, $(Ka_o)^2$ has a minimum at $\theta = 0$ and a maximum at $\theta = \pi$. For $E_n/E \ll 1$ (Born approximation), one obtains from Eq. (17)

$$(Ka_o)_{min}^2 = \frac{E_n^2}{4RE}\left[ 1 + \frac{1}{2}\left(\frac{E_n}{R}\right) + O\left(\left(\frac{E_n}{E}\right)^2\right) \right] \tag{18}$$

$$(Ka_o)_{max}^2 = 4\left(\frac{E}{R}\right)\left[ 1 - \frac{1}{2}\left(\frac{E_n}{E}\right) + O\left(\left(\frac{E_n}{E}\right)^2\right) \right] \tag{19}$$

For excitation to continua (e. g., ionization), the excitation energy is no longer a discrete variable but is a continuous variable $E'$ taking all real values greater than the first ionization threshold $I_1$. Now, the cross section (at a fixed E) for excitation to continuum states between $E'$ and $E' + dE'$ is $(d\sigma/dE')dE'$, and $d\sigma/dE'$ is the density of the cross section per unit range of $E'$. Alternatively, $\sigma(E')$ may be considered as the cross section for excitation to all states up to $E'$ and $d\sigma/dE'$ as the derivative of $\sigma(E')$. Thus Eq. (15) may be adapted to give the differential of $d\sigma/dE'$ as

$$d\left(\frac{d\sigma}{dE'}\right) = \frac{4\pi a_o^2}{E/R} \frac{R}{E'} \frac{df(K,E')}{dE'} d[\ell n(Ka_o)^2] \tag{20}$$

The density of the generalized oscillator strength per unit range of $E'$, $df(K, E')/dE'$, is defined by

$$df(K,E')/dE' = \sum_n (E_n'/R)\left[|\epsilon_n(K)|^2/(Ka_o)^2\right]\delta(E_n - E') \tag{21}$$

where the summation runs over all excited states—discrete as well as continuum.

It is well known from quantum mechanical perturbation theory that the probability for a transition from a state m to a state n is proportional to the factor

$$|\langle n|e^{i\vec{k}\cdot\vec{r}}\hat{n}\cdot\vec{p}|m\rangle|^2 = |\int\psi_n^* e^{i\vec{k}\cdot\vec{r}}\hat{n}\cdot\vec{p}\psi_m d\vec{r}|^2 \tag{22}$$

where the $\psi$'s are the atomic eigenfunctions, $\vec{k}$ is the wave propagation vector, and $\hat{n}\cdot\vec{p}$ is the component of the electron momentum $\vec{p}$ along the direction of polarization of the incident radiation, i.e., the direction of the electric field vector. Usually the wavelength of the emitted or absorbed radiation is much greater than the dimensions of the atom, whereas the wave functions are nonvanishing only in a region of the size of the atom. Thus, the quantity $\vec{k}\cdot\vec{r}$ in Eq. (22) is small compared to unity and from the expansion

$$e^{i\vec{k}\cdot\vec{r}} = 1 - i(\vec{k}\cdot\vec{r}) + \frac{[-i(\vec{k}\cdot\vec{r})]^2}{2!} + \cdots \tag{23}$$

we can replace exp $(i\vec{k} \cdot \vec{r})$ by 1. The probability for a transition from a state m to a state n is then approximately proportional to

$$P_{nm} \propto |<n| \hat{n} \cdot \vec{p} |m>|^2 = |\hat{n} \cdot <n|\vec{p}|m>|^2 \qquad (24)$$

If the matrix element in Eq. (24) vanishes, the second term in the expansion (Eq. (23)) must be considered. By using the unperturbed Hamiltonian and the commutation relations for momentum and coordinate operators, it can be shown in general that the matrix element of the momentum operator in Eq. (24) can be replaced by the matrix element of the coordinate. As the dipole moment is usually defined by $e <n|\vec{r}|m>$, it follows that the probability for a transition from a state m to a state n is proportional to the dipole-matrix-element squared, i.e.,

$$P_{nm} \propto |\hat{n} \cdot <n|\vec{r}|m>|^2 \qquad (25)$$

For a multi-electron atom, Eq. (25) becomes

$$P_{nm} \propto |<n|\vec{M}|m>|^2 \qquad (26)$$

where $\vec{M}$ is a vector with components

$$\sum_{j=1}^{Z} e_j x_j, \quad \sum_{j=1}^{Z} e_j y_j, \quad \text{and} \quad \sum_{j=1}^{Z} e_j z_j$$

and the atomic eigenfunctions are denoted by $|n> = |S> |L> |n>$ and $|m> = |S_o> |L_o> |n_o>$ for L-S coupling and by $|n> = |J> |n>$ and $|m> = |J_o> |n_o>$ for J-J coupling. The total quantum numbers $(n, n_o)$ identify the final and initial electronic states, respectively. The existance of nonvanishing values of the dipole-matrix-element of Eq. (26) determines the selection rules for electric dipole radiation. If either type of coupling is assumed, the selection rule for the total angular momentum is $\Delta J = 0, \pm 1$ with the restriction that $J = 0 \rightarrow J = 0$ is not permitted. In addition, the initial and final states must have opposite parity. For L-S coupling, there is a strong interaction between individual electronic spin and orbital angular momentum vectors to give the resultant L and S with the selection rules $\Delta S = 0$, and $\Delta L = 0, \pm 1$. For J-J coupling, which is generally prevalent for large Z species, there is a strong interaction between the spin and orbital angular momenta of the individual electron giving the resultant total electronic angular momentum J with the selection rule $\Delta J = 0, \pm 1$ for the electron whose state is changed.

Transitions which obey the selection rules described above are called electric dipole or optically allowed transitions, whereas those transitions which violate these rules are optically forbidden. If both the initial and final state wavefunction are spherically symmetric, the integral in Eq. (22) is identically zero, and transitions between these states are strictly forbidden. The selection rules for forbidden transitions can be determined by evaluating the matrix elements obtained by including the second term of the expansion Eq. (23). Note that the selection rules presented here are all first order in that the probability for the transition was obtained from first-order perturbation theory.

### 1.2.2 Integrated Cross Section

The cross section for excitation to a specific state n of an atom or molecule, regardless of the angle of scattering of an incident particle, is defined as the integrated cross section of the transition. For the nonrelativistic case, $\sigma_n$ is simply an integral of $d\sigma_n$, as given by Eq. (15), over all kinematically possible values of the momentum transfer $\hbar K$, i.e.,

$$\sigma_n = \frac{4\pi a_o^2}{E/R} \int_{(Ka_o)^2_{min}}^{(Ka_o)^2_{max}} \frac{f_n(K)}{E_n/R} \frac{d(Ka_o)^2}{(Ka_o)^2} \tag{27}$$

where $(Ka_o)^2_{min}$ and $(Ka_o)^2_{max}$ are given by Eq. (18) and Eq. (19), respectively.

Since the Born approximation assumes sufficiently large incident electron kinetic energy, Bethe recognized the usefulness of expressing the cross section in terms of an asymptotic expansion in inverse powers of electron kinetic energy. To explain the general features of the asymptotic expansion, we consider the generalized oscillator strengths of the optically allowed helium $2^1P$ excitation (Ref. 2). A plot of $f_n(K)/(E_n/R)$ versus $\ln (Ka_o)^2$ is given in Fig. 1. The integral in Eq. (27) is represented by the area under the curve limited by $\ln (Ka_o)^2_{min}$ and $\ln (Ka_o)^2_{max}$. Because the integrand decreases rapidly for large values of $(Ka_o)^2$, for large values of E, the upper limit of the integration may be accurately taken as being infinite. Further, $(Ka_o)^2_{min}$ in in general small and decreases with increasing E. Now choose the value $(Ka_o)^2$ such that the areas ABC and CDF in Fig. 1 are equal. Thus it becomes obvious that the required area is given in the Born approximation (large E) by the product of $\ln (\overline{K}a_o)^2 - \ln (Ka_o)^2_{min}$

and the dipole-matrix-element squared $M_n^2 = f_n R/E_n$ which is defined by Eqs. (12) and (13). Analytically,

$$\ell n(\bar{K}a_o)^2 = \int_o^\infty \frac{f_n(K)}{f_n} \, d[\ell n(Ka_o)^2] - \int_{-\infty}^o \left[ 1 - \frac{f_n(K)}{f_n} \right] d[\ell n(Ka_o)^2] \tag{28}$$

Thus, $(\bar{K}a_o)^2$ is independent of E, and Eq. (27) becomes

$$\sigma_n = \frac{4\pi a_o^2}{E/R} \int_{\ell n(Ka_o)^2_{min}}^{\ell n(Ka_o)^2_{max}} \frac{f_n(K)}{F_n/R} \, d[\ell n(Ka_o)^2]$$

$$= \frac{4\pi a_o^2}{E/R} \left\{ M_n^2 \, \ell n \left[ \frac{(\bar{K}a_o)^2}{(Ka_o)^2_{min}} \right] + O\left(\frac{E_n}{E}\right) \right\}$$

$$= \frac{4\pi a_o^2}{E/R} \left\{ M_n^2 \, \ell n \left[ (\bar{K}a_o)^2 \left(\frac{4RE}{F_n}\right) \right] + O\left(\frac{E_n}{E}\right) \right\} \tag{29}$$
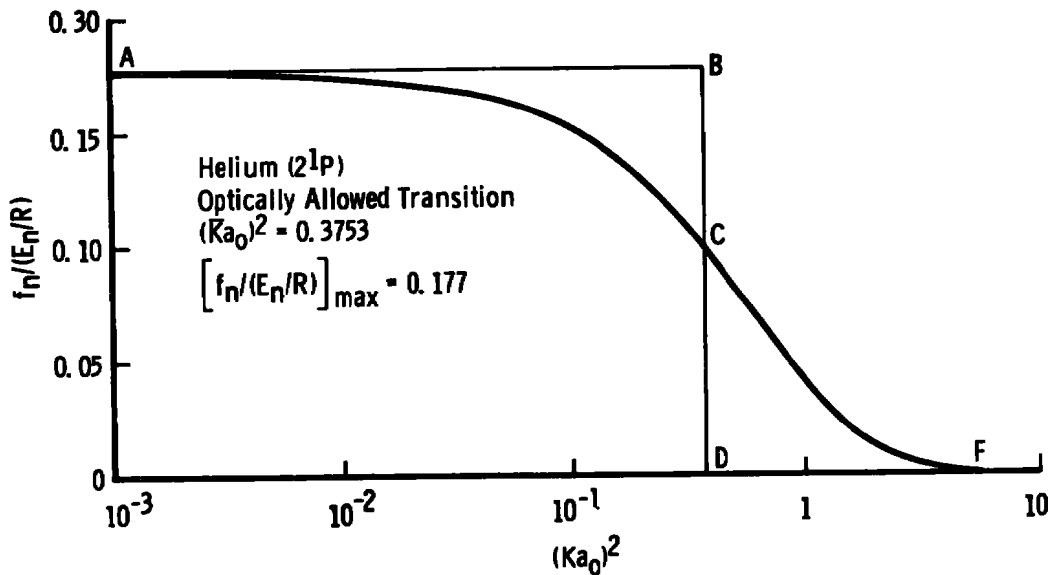


Figure 1. Momentum dependence of the generalized oscillator strength for the optically allowed helium $2^1 P$ excitation.

Following the practice of other authors in recent years, we define

$$\ln C_n = \ln\left[(\bar{K}a_o)^2\left(\frac{4R}{E_n}\right)\right] \qquad (30)$$

Consequently, the Bethe asymptotic formula for optically allowed excitation by electron impact is given by

$$\sigma_n = \frac{4\pi a_o^2 R}{E} M_n^2 \ln(C_n E) \qquad (31)$$

The optically forbidden excitation, for which $f_n = 0$, follows in an obvious manner. A plot of $f_n(K)/(E_n/R)$ versus $\ln(Ka_o)^2$ for the helium $(2^1S)$ excitation is shown in Fig. 2. The asymptotic cross section for optically forbidden excitations is simply

$$\sigma_n = \frac{4\pi a_o^2 R}{E} b_n \qquad (32)$$

where $b_n$ is defined by

$$b_n = \int_{-\infty}^{+\infty} \frac{f_n(K)}{E_n/R} d[\ln(Ka_o)^2] \qquad (33)$$

Note that the constants $b_n$ and $C_n$ are each properties of the respective transition to state n and depend upon the excitation energy $E_n$.
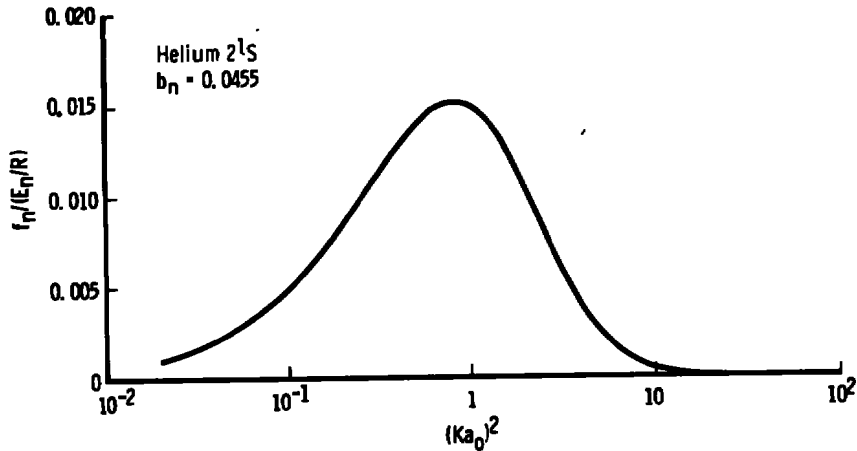


Figure 2. Momentum dependence of the generalized oscillator strength for the optically forbidden helium $2^1S$ excitation.

For excitation to continua, the integrated cross section $d\sigma/dE'$ per unit range of excitation energy $E'$, using the differential generalized oscillator strength $df(K, E')/dE'$ in place of $f_n(K)$, is defined by an equation similar to Eq. (27). The Bethe procedure then leads to

$$\frac{d\sigma}{dE'} = \left(\frac{4\pi a_0^2}{E/R}\right)\left(\frac{R}{E'}\right)\left(\frac{df}{dE'}\right) \ell n(C_{E'} \cdot E)$$

(34)

where $df/dE' = [df(K, E')/dE']_{K=0}$ is the differential optical oscillator strength and $C_{E'}$ is defined by Eqs. (28) and (30) after replacement of $f_n(K)$ by $df(K, E')/dE'$.

The ionization cross section for an atom, which is obtained by integrating Eq. (34) over the continuum energy $E'$, is given by

$$\sigma_i = \left(\frac{4\pi a_0^2 R}{E}\right) M_i^2 \ell n(C_i E)$$

(35)

where

$$M_i^2 = \int_{I_1}^{\infty} \eta(E')\left(\frac{R}{E'}\right)\left(\frac{df}{dE'}\right) dE'$$

(36)

and

$$M_i^2 \ell n C_i = \int_{I_1}^{\infty} \eta(E')\left(\frac{R}{E'}\right)\left(\frac{df}{dE'}\right) \ell n\, C_{E'} dE'$$

(37)

The quantity $M_i^2$, which is related to the distribution of the optical oscillator strength, is called the effective dipole-matrix-element squared for ionization. Since various processes can occur as a result of energy transfer $E'$ in a single collision, the quantities $M_i^2$ and $C_i$ are expressed containing $\eta(E')$, which is defined as the efficiency for ionization at excitation energy $E'$.

### 1.2.3 Molecular Excitation Cross Sections

When applying the differential cross section formula Eq. (15) to molecules, the symbol o or n represents a set of quantum numbers (electronic, vibrational, and rotational) which designates a molecular state, and the quantity $|\epsilon_n(K)|^2$ requires further specification to include the molecular internal degrees of freedom. For a diatomic molecule,

18

the final state is specified by the electronic quantum number n, vibrational quantum number v, and rotational quantum numbers J and M, with corresponding initial state quantum numbers $n_0$, $v_0$, $J_0$, and $M_0$. By assuming the Born-Oppenheimer separation between the electronic and nuclear motions and neglecting the rotational-vibrational coupling, the final state wave function is

$$\Psi_{nvJM} = \xi_n(\vec{r}_i,\vec{\rho})\chi_{nv}(\rho)Y_{JM}(\Theta,\Phi)$$

(38)

and that of the initial state is

$$\Psi_{n_0 v_0 J_0 M_0} = \xi_{n_0}(\vec{r}_i,\vec{\rho})\chi_{n_0 v_0}(\rho)Y_{J_0 M_0}(\Theta,\Phi)$$

(39)

where the $\xi$'s are electronic wavefunctions depending on the coordinate $\vec{r}_i(i = 1, 2, \ldots Z)$ of all the molecular electrons and on the nuclear coordinates $\vec{\rho}(\rho, \Theta, \Phi)$, the $\chi$'s are the vibrational wavefunctions depending on the internuclear distance $\rho$, and the Y's are spherical harmonics. The form factor for the transition is then given by

$$\epsilon(K;n,v,J,M \leftarrow n_0,v_0,J_0,M_0) = \int \chi_{nv}^*(\rho)Y_{JM}^*(\Theta,\Phi)\epsilon_n(K;\rho,\Theta,\Phi)\chi_{n_0 v_0}(\rho)Y_{J_0 M_0}(\Theta,\Phi)\rho^2 d\rho d(\cos\Theta)d\Phi$$

(40)

where $\epsilon_n(K;\rho, \Theta, \Phi)$ is the electronic part defined by

$$\epsilon_n(K;\rho,\Theta,\Phi) = \int \xi_n^*(\vec{r}_i,\vec{\rho}) \sum_{j=1}^{Z} \exp(i\vec{K} \cdot \vec{r}_j)\xi_{n_0}(\vec{r}_i,\vec{\rho})d^Z\vec{r}_i$$

(41)

Since rotational level spacings of molecules are much smaller than the energy resolution of most collision experiments, they are treated as effectively degenerate and, therefore, summed over all J and M and averaged over $J_0$ and $M_0$. The resulting squared form factor for the transition from the vibrational level $v_0$ in the initial electronic state $n_0$ to the vibration level v in the final electronic state n is then obtained by using the closure property of spherical harmonies as

$$|\epsilon_n(K;v \leftarrow v_0)|^2 = (4\pi)^{-1} \iint d(\cos\Theta)d\Phi \left| \int \chi_{nv}^*(\rho)\epsilon_n(K;\rho,\Theta,\Phi)\chi_{n_0 v_0}(\rho)\rho^2 d\rho \right|^2$$

(42)

Note this result shows that $|\epsilon_n(K;v \leftarrow v_0)|^2$ is equal to the average of the squared form factor evaluated for all possible molecular orientations.

19

Since $\epsilon_n(K;\rho, \Theta, \Phi)$ is generally a more slowly varying function of $\rho$ than are the vibrational wave functions, $\epsilon_n(K;\rho, \Theta, \Phi)$ may be replaced by its value $\epsilon_n(K;\overline{\rho}, \Theta, \Phi)$ at a representative $\rho$ value of $\overline{\rho}$, which may be taken as the equilibrium internuclear distance $\rho_e$ if $v_o = 0$. Physically, this means that the nuclei do not move appreciably in the period during which electrons undergo a transition under the influence of the incident electron. Thus, Eq. (42) becomes

$$|\epsilon_n(K;v \leftarrow v_o)|^2 = (4\pi)^{-1} \iint d(\cos\Theta)d\Phi |\epsilon_n K;\overline{\rho},\Theta,\Phi)|^2 |\int X_{nv}^*(\rho)X_{n_o v_o}(\rho)\rho^2 d\rho|^2 \qquad (43)$$

Note that the first factor in Eq. (43) deals primarily with the electronic motion, and thus may be called the electronic form factor squared; whereas the second deals exclusively with the nuclear vibration and is identical to the Franck-Condon factor and is well known in molecular spectroscopy. Applications of the Franck-Condon principle will be shown later in this section.

The differential cross section equation for molecular electron excitation to state n is the same as in the atomic case (Eq. (15)) with the form factor in the generalized oscillator strength (Eq. (11)) redefined by Eq. (43) and n redefined to include the entire set of molecular quantum numbers. Applying this reinterpretation of the form factor and n to Eq. (20) gives the differential of the cross-section density per unit range of E' for excitation to continua.

The integrated cross section for molecular excitation to state n, where n contains the required set of molecular quantum numbers, is given by Eq. (27) if the generalized oscillator strength, or the form factor, is redefined by Eq. (43). The Bethe procedure then leads to an equation identical in form to Eq. (31) for optically allowed transitions and to Eq. (32) for optically forbidden transitions. The selection rules for these transitions are obtained just as in the atomic case by evaluating the matrix elements of the electric dipole moment and are described in detail by Herzberg (Ref. 3).

For excitation to continua, the integrated cross section $d\sigma/dE'$ per unit range of excitation energy E', using the reinterpreted differential generalized oscillator strength for molecular processes $df(K, E')/dE'$ instead of $f_n(K)$, is defined by an equation similar to Eq. (27). The Bethe procedure then leads to an equation identical in form to Eq. (34) for excitation to continua.

For an atom, excitation is generally to a specific state by an allowed or forbidden transition or to continua as an ionization process

with integrated cross sections described by Eq. (31), (32), and (35), respectively. For a molecule, additional excitation channels are open for each electron-molecule collision; these can be summarized by three basic diagrams that also serve to illustrate the consequence of the Franck-Condon principle (Ref. 3). In Fig. 3, the lower curves represent the initial state of the molecule. By assuming the Franck-Condon principle, the transition takes place so quickly that the nuclei do not have time to move an appreciable distance, and since the nuclear separation in the lower vibrational level will effectively lie between a and b, the upper state of the molecule will be represented by points lying between c and d on the upper curve.
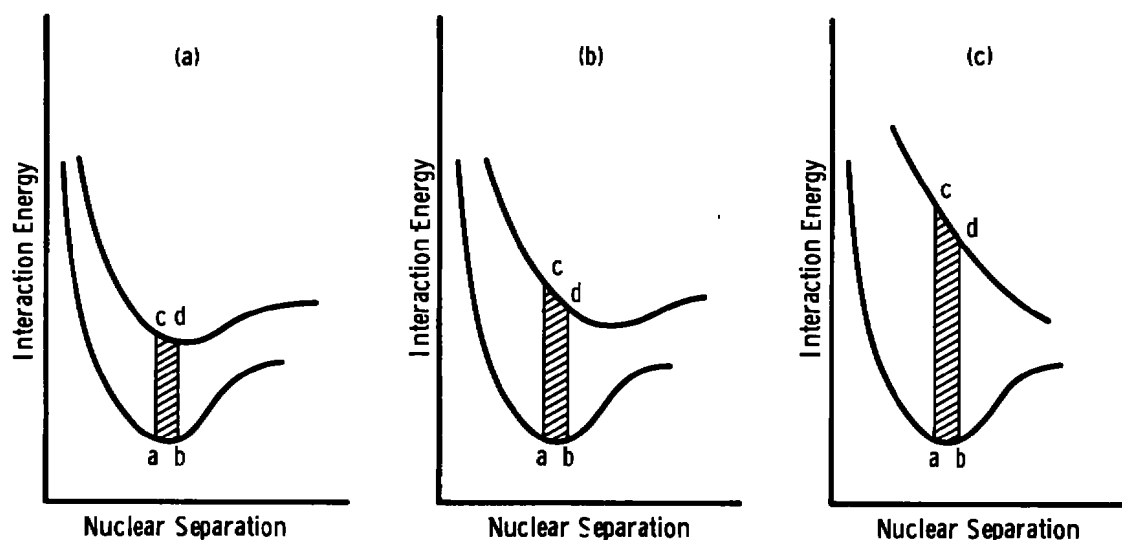


Figure 3. Molecular electronic transitions illustrating the consequences of the Franck-Condon principle.

Figure 3a illustrates excitation to a stable molecular state, and Fig. 3c shows excitation to continua resulting in dissociation of the molecule, while Fig. 3b is a mixture of excitations leading to stable molecules and to dissociation. Similarly, ionization of a molecule can be described using Fig. 3 where the upper potential energy curve corresponds to an electronic state of the molecular ion. When atomic excitations resulting from the dissociation of a molecule are of interest, many more excitation channels become available thus further complicating the analysis.

Fortunately, these many types of molecular excitations can be described by relatively few equations. For optically allowed excitations, the integrated cross section is given by

$$\sigma_n = \frac{4\pi a_0^2 R}{E} M_n^2 \ln(C_n E)$$ (44)

which is identical in form to Eq. (31) for atomic processes. For excitation to a stable molecular state n, $M_n^2$ is related to the optical oscillator strength $f_n$ by $M_n^2 = f_n(R/E_n)$ where $E_n$ is the excitation energy. In the case of dissociative excitation to the atomic state n, $M_n^2$ is related to the optical oscillator strengths of all dipole transitions to molecular states which lead to formation of the particular state n and is given by

$$M_n^2 = \int_{E_n}^{\infty} \eta_n(E')\left(\frac{R}{E'}\right)\left(\frac{df}{dE'}\right) dE'$$ (45)

where $E'$ is the excitation energy transferred to the molecule, $E_n$ is the threshold energy for the process under consideration, $\eta_n(E')$ is the probability that the intermediate molecular states will dissociate into the particular atomic state n, and $df/dE'$ is the differential optical oscillator strength. The remaining coefficient $C_n$ in the cross-section formula is obviously defined by

$$M_n^2 \ln C_n = \int_{E_n}^{\infty} \eta_n(E')\left(\frac{R}{E'}\right)\left(\frac{df}{dE'}\right) \ln C_{E'} dE'$$ (46)

For ionization, the factor $\eta_n(E')$ need only be redefined as the probability that the molecule ionizes upon receiving an energy transfer $E'$.

For optically forbidden excitations, the integrated cross section is given by

$$\sigma_n = \frac{4\pi a_0^2 R}{E} b_n$$ (47)

where $b_n$ is a constant related by Eq. (33) to the generalized oscillator strength defined in terms of the molecular form factor. In the case of dissociative excitation to the atomic state n, $b_n$ is a constant depending on the sum of all optically forbidden processes leading to formation of atoms in state n.

Whenever the cross sections are plotted in the form $\sigma E/(4\pi a_0^2 R)$ versus $\ln E$ (Bethe plot), the optically allowed, optically forbidden, and spin forbidden excitations have curves with positive, zero, or negative

slope, respectively. The slopes of these lines are related to $M_n^2$ and the intercepts to $C_n$. It is generally found that for optically allowed processes $C_n$ has a value near one and for optically forbidden processes $C_n \gg 1$ (Ref. 4).

In summary, to enable the knowledgeable design of electron beam systems for investigations of flow fields of such binary mixtures as $N_2$/He and $N_2$/NO, it is desired to experimentally determine the functional dependence on energy (see Eqs. (44) and (47)) of various dissociative excitation processes of electron-$N_2$ and -NO collisions. Further, the variation of the electron-beam-induced fluorescence intensity with both beam current and molecular specie density is to be investigated under such experimental conditions as to preclude collisional quenching effects. The experimental apparatus used for these purposes is described in the following section.

## 2.0 EXPERIMENTAL APPARATUS

### 2.1 VACUUM CHAMBER AND GAS SUPPLY

The vacuum chamber was a stainless steel cylindrical vessel of 26.5 cm inside diameter and 45 cm length. Interior to the vacuum chamber was installed a cylindrical copper cooling liner which was aligned both axially and radially with the vacuum chamber. The cooling liner was of 22 cm inside diameter, extended the length of the vacuum chamber, and was held in place by several set screws. The cooling liner had three 2.5-cm-diam access ports, one of which was used for the electron-beam injection orifice. The remaining two ports were available for optical detection of the electron-beam fluorescence and were aligned with the quartz optical window of the vacuum chamber. The vacuum chamber was essentially that of Ref. 5.

The copper liner temperature was determined by a copper-constantan thermocouple attached to the liner, and the observed variation of liner temperature was less than 0.5 K.

Chamber pumping was provided by a 10.2-cm-diam oil diffusion pump with a water-cooled baffle, providing chamber pressures of less than $10^{-6}$ torr. The baffle cooling source was later changed from water to a Freon® refrigerator to further reduce diffusion pump backstreaming. The chamber pressure was controlled by varying the mass flow rate

through the system using both a needle valve and a Granville-Phillips leak valve at the inlet of the gas to the chamber and also by adjusting the gate valve opening to the 10.2-cm diffusion pump at the chamber exit.

An NRC Model 820 Alphatron® gage monitored the pressure at a point between the copper liner and chamber wall; a calibrated MKS Baratron was used to determine the scattering cell pressure for the relative intensity measurements.

The mechanical pump exhaust was vented to the atmosphere through a 1.27-cm-diam copper tube. To avoid back pressure on the mechanical pump and to dilute the concentration of NO in the vent tube, an injector nozzle was attached to the pump vent connection, and high-pressure dry nitrogen was used to purge the venting tube.

## 2.2 ELECTRON GUN SYSTEM

The electron gun, which was the same as used for the measurements reported in Ref. 5, was a television type, oxide-coated cathode model and typically provided a steady 1.5- to 3.0-mA current for 10 to 30 hr. A Universal Voltronics high-voltage power supply with a 0.01-percent ripple filter provided a negative potential of 4 to 20 kV to the electron gun cathode. The high voltage power supply, which was calibrated using a secondary standard Weston ammeter and calibrated $M\Omega$ resistors, had an error of less than 5 percent between 4 and 7 kV and less than 2 percent above 7 kV as shown in Fig. 4. The filament and accelerator power supply shown in Fig. 5 was designed to replace batteries used previously and to allow immersion in oil, which permitted operation up to 50 kV without arcing and corona effects.

Magnetic coils situated near the electron gun cathode provided for electron beam focus at and deflection about the 1.3-mm-diam orifice, which was situated approximately 56 cm from the gun cathode and located just interior to the vacuum chamber as shown in Fig. 6. A 10.2-cm oil diffusion pump with a water-cooled, and later Freon-refrigerator-cooled, baffle maintained the differentially pumped drift tube section at a pressure of less than $10^{-5}$ torr when the chamber pressure was $2 \times 10^{-3}$ torr.
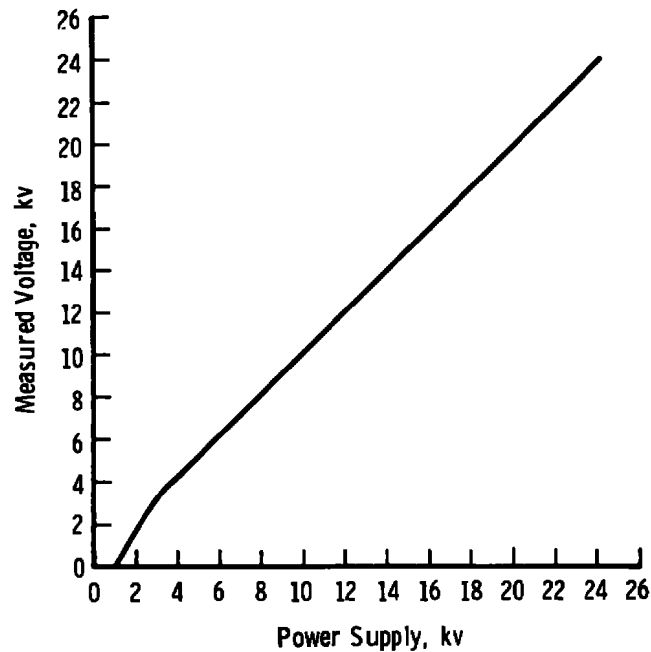
Figure 4. Calibration of Universal Voltronics high voltage power supply.
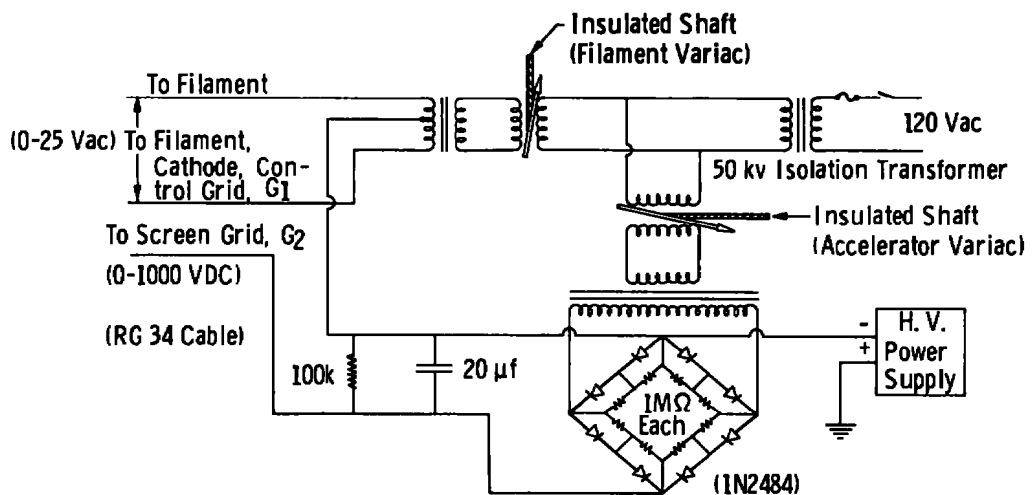


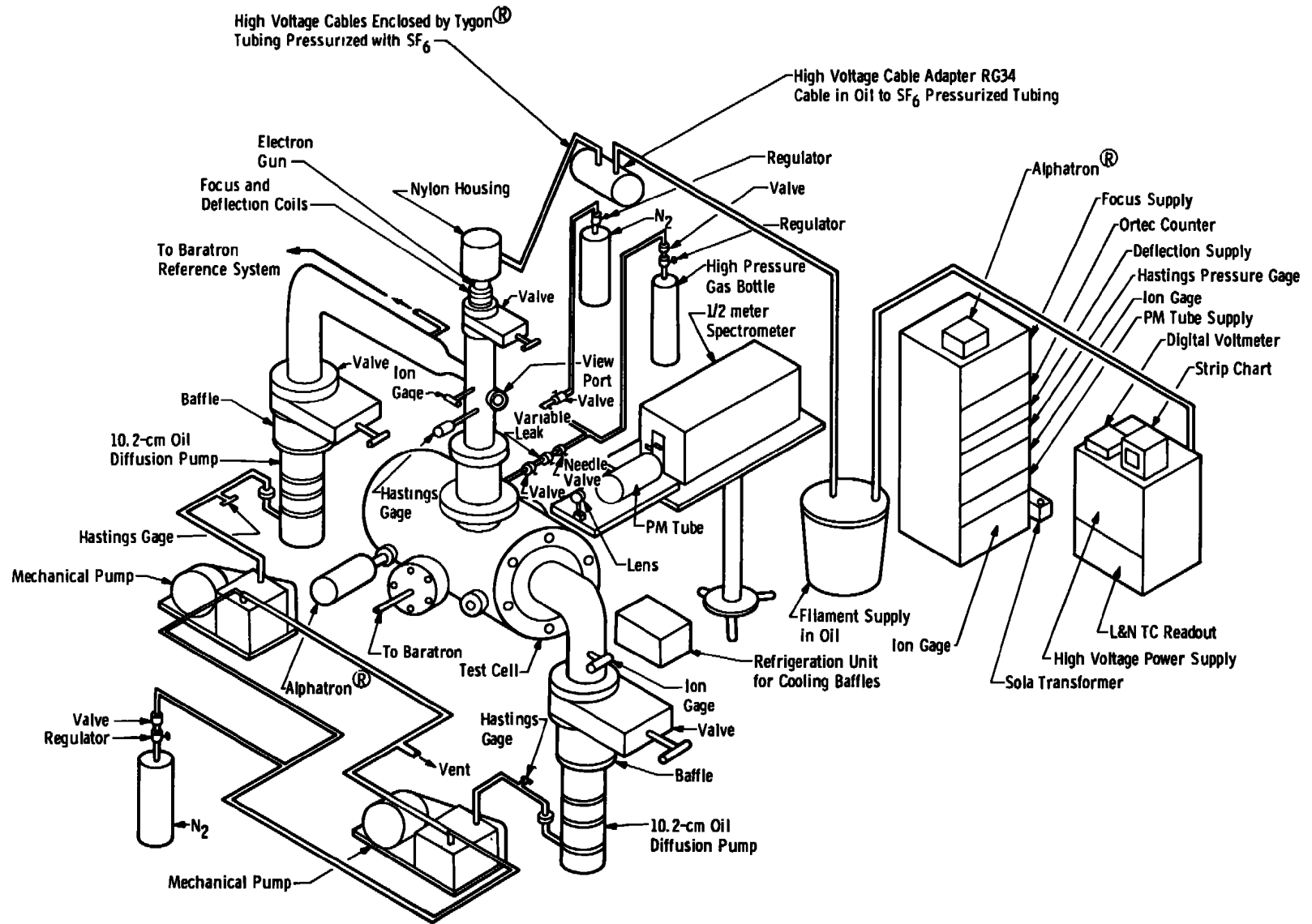Figure 5. Electron gun filament and accelerator power supply.

Figure 6. Experimental system.

The electron beam Faraday cup collector consisted of a water-cooled, 4.1-cm-diam right-angle elbow copper cylinder and two screen grids with 1.9-cm-diam entrance holes, the second of which was biased at -30 v for the suppression of secondary electrons. The initial collecting surface was inclined at an angle of 45 deg to the beam direction and, therefore, extended from 2.5 to 4.1 cm below the top grid. Measuring from the center of the inclined surface, the cylinder extended 12.7 cm to collect scattered electrons. This particular configuration of the Faraday cup was necessary to provide, within the space limitations of the chamber, an adequate length-to-diameter ratio of the collector to minimize reflective loss of the electron beam on inpact with the collector. The interior surfaces of the Faraday cup were coated with Aquadag®, a colloidal graphite suspension. The beam current collected by the Faraday cup was determined by measuring the potential drop across a 10-k$\Omega$ resistor with an NLS Model 481 digital voltmeter, which was later replaced with a Heathkit Model IM-102 multimeter.

## 2.3 OPTICS AND DETECTORS

The optical arrangement employed for these measurements is shown in Fig. 6. The 10-cm-diam glass lens had a focal length of 25.54 cm, and the overall optical magnification of the system was 1.0. A 0.5-m Jarrell Ash scanning spectrometer was employed with an 1180-groove/mm grating blazed at 5000 Å, and the reciprocal linear dispersion was 16 Å/mm. The spectrometer was mounted on its side with the entrance slit of the spectrometer imaged onto the chamber centerline such that the slit length was perpendicular to the electron beam direction.

An EMI 6256S photomultiplier tube of S-11 spectral response was used, and the operating voltage of 1500 v was supplied by a Fluke Model 405B, high-voltage power supply. The photomultiplier tube temperature was maintained near -32°C, using gaseous $N_2$ cooling, for the purposes of reducing the dark count and increasing the overall signal-to-noise ratio of the tube (Refs. 6 and 7). The dark count was normally one count per second at this operating temperature.

The relative spectral sensitivity of the system was determined by placing a GE 30A-T24-17 tungsten strip lamp at the observation volume and recording the system response as a function of wavelength. The spectral radiance $N_\lambda(\lambda, T_B)$ of the lamp operating at a true lamp temperature T with emissivity $\epsilon(\lambda, T)$ and lamp transmissivity $\tau$ is given by

$$N_\lambda(\lambda, T_B) = \tau \epsilon(\lambda, T) N_\lambda(\lambda, T), \text{ watts/cm}^2\text{-sr-cm} \tag{48}$$

or in terms of the photon rate

$$N_\lambda'(\lambda, T_B) = N_\lambda(\lambda, T_B)/(h\lambda/c) \tag{}$$

where $\lambda$ is the wavelength of the radiation and $T_B$ is the brightness temperature of the lamp. It is seen from Eq. (48) that $T_B$ is the temperature of a blackbody which emits the same radiant intensity at $\lambda$ as does the tungsten surface at temperature T.

Using the Planck radiation law the spectral radiance is given by

$$N_\lambda(\lambda, T_B) = C_1 \lambda^{-5}[\exp(C_2/\lambda T_B) - 1]^{-1}, \text{ watts/cm}^2\text{-sr-cm} \tag{49}$$

By assuming large values of $C_2/\lambda T_B$, one can write Eq. (49) in the Wien law approximation as

$$N_\lambda(\lambda, T_B) = C_1 \lambda^{-5} \exp[-C_2/\lambda T_B] \tag{50}$$

Consequently, Eq. (48) becomes

$$C_1 \lambda^{-5} \exp(-C_2/\lambda T_B) = \tau \epsilon(\lambda, T) \cdot C_1 \lambda^{-5}[\exp(C_2/\lambda T) - 1]^{-1} \tag{51}$$

By using the Wien law approximation, Eq. (51) can be written as

$$1/T = 1/T_B + (\lambda/C_2) \ln[\tau \epsilon(\lambda, T)] \tag{52}$$

The emissivity data of DeVos (Ref. 8) show that, for $\lambda = 6500$ Å, the pyrometer wavelength $\epsilon(650 \text{ nm}, T)$ can be written as

$$\epsilon(650 \text{ nm}, T) = \epsilon(650 \text{ nm}, 2400) + [(T - 2200)/200][\epsilon(650 \text{ nm}, 2200) - \epsilon(650 \text{ nm}, 2400)] \tag{53}$$

for $2200 \leq T \leq 2400$ K. Since $\tau$ for the fused silica strip lamp window is known to be 0.93 (Ref. 9), Eqs. (52) and (53) can be solved iteratively for the true lamp temperature T once the brightness temperature is determined using a pyrometer. Using the true temperature T produces the spectral radiance of the lamp of

$$N_\lambda = r\epsilon(\lambda,T) \cdot C_1\lambda^{-5}[\exp(C_2/\lambda T) - 1]^{-1} \tag{54}$$

The constants $C_1$ and $C_2$ are

$$C_1 = 1.1909 \times 10^{-12}, \text{ watt-cm}^2/\text{sr}$$

$$C_2 = 1.4380 \quad , \text{ cm-K}$$

The relative spectral sensitivity $S(\lambda)$ of the system is defined as the ratio of the system response $I^{rel}_{(\lambda)}$ normalized by the lamp radiance $N_\lambda$ and the maximum value of $I^{rel}_{(\lambda)}/N_\lambda$ for the spectral range studied; i.e.,

$$S(\lambda) = [I^{rel}_{(\lambda)}/N_\lambda]/[I^{rel}_{(\lambda)}/N_\lambda]_{max} \tag{55}$$

The relative spectral sensitivity $S(\lambda)$ was determined by performing relative intensity measurements of the lamp output at 50-Å intervals over the spectral range of 3500 to 6550 Å using 200-$\mu$m spectrometer slit widths and two neutral density filters of known transmission factors. The strip lamp was powered by an EG and G Model 590-11 power supply operated at 30 amp and 6 v. This supply provides a chopper-stabilized, 1-kHz square-wave output which is feedback regulated to within 0.25 percent rms of the selected value which provides control of the lamp output to within 1 percent. A calibrated L and N optical pyrometer was used to determine the brightness temperature $T_B$ of the lamp which was 2141 ± 6 K for these calibrations. An iterative computer calculation was used for Eqs. (52) to (54) to determine $S(\lambda)$ given by Eq. (55), and $S(\lambda)$ for the system as shown in Fig. 7. It is estimated that the relative $S(\lambda)$ values are determined to within an inaccuracy of 1 to 2 percent.

## 2.4 PHOTON COUNTING SYSTEM

The photon counting system, which was the same as that reported in Ref. 5, consisted of the following ORTEC apparatus: Model 454 Timing Filter Amplifier, Model 436 100 MHz Discriminator, and Model 715 Dual Counter/Timer. Figure 8 shows a block diagram of the system.
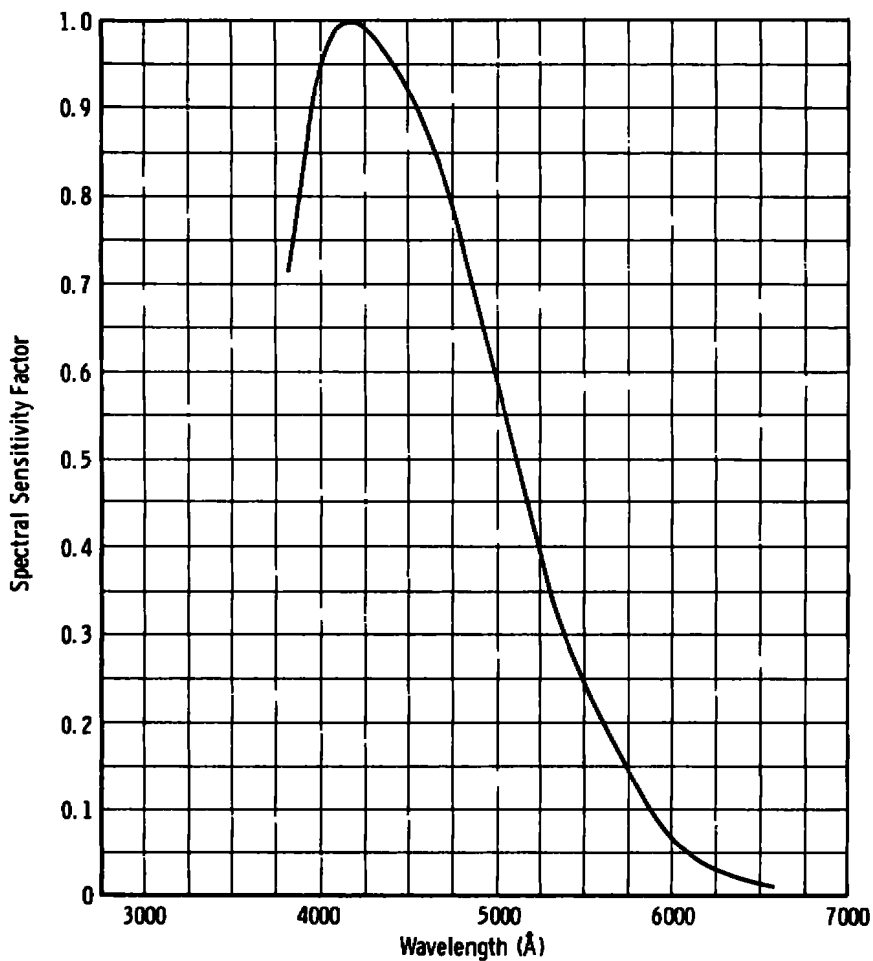
Figure 7. Relative spectral response of the system.
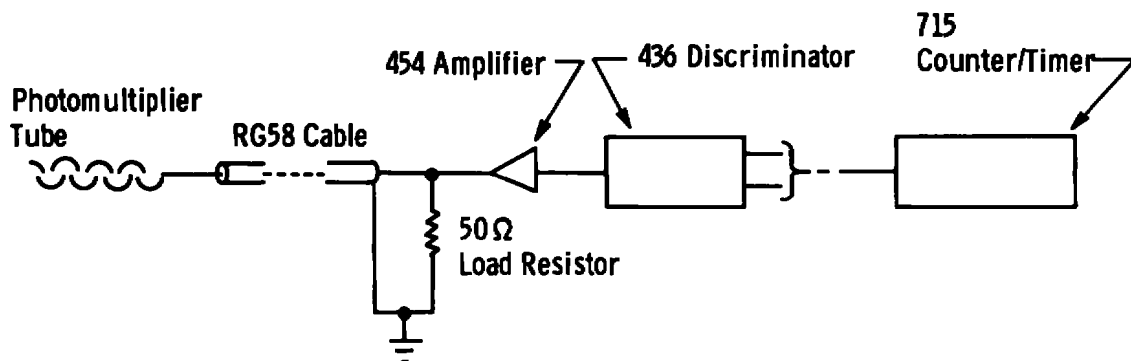


Figure 8. Block diagram of ORTEC photon counting system.

The 715 counter/timer includes dual counters, one of which, in conjunction with a precise internal oscillator, may be preset for an accurate counting interval so that the system can be used as a discrete rate meter. The output is available as either positive or negative pulses. The negative output is passively shaped to an extent determined by the time constant selection, but it is required only for extremely high rate applications. The positive pulse is a standardized pulse of +5 v and 0.5 $\mu$sec width. The 715 counter has a frequency response of 20 MHz and an approximate dead-time of 50 nsec. The counter/timer will accept either discriminator output, and for this report, the negative output was used for the measurements that were made. The discriminator was operated at 0.6 v for the purpose of excluding dark counts and obtaining the highest signal-to-noise ratio of the system (Ref. 10).

## 3.0 RESULTS AND ANALYSIS

Preliminary to the cross-section measurements, atomic line spectral profile data were acquired using 100-$\mu$m slit widths giving a spectral bandpass of 1.6 Å in order to isolate spectral impurities and determine appropriate slit widths. Since the slit length was perpendicular to the beam, the photon count rate was proportional to the slit width, and increasing the slit width pays handsome dividends. The spectral line profiles were determined by measuring the radiative photon rate of each transition as a function of wavelength. Figures 9 through 12 show the spectral features of NII($N_2$; 5016.4 Å), NII(NO; 5016.4 Å), NII($N_2$; 3995.0 Å), and NII(NO; 3995.0 Å), respectively. The data were acquired at a beam energy of 10 keV, except for NII($N_2$; 3995.0 Å) which was at 7 keV, and the pressures and currents were: 8.35 mtorr, 860 $\mu$A; 5.3 mtorr, 745 $\mu$A; 2.8 mtorr, 220 $\mu$A; and 5.5 mtorr, 725 $\mu$A, respectively.

The NII($N_2$; 3995.0 Å) spectral impurity is due to the $N_2$(2+)(1,4) band at 3998.4 Å (Ref. 11). By using the peak cross sections for the $N_2$(2+)(1,4) band (Ref. 12), the secondary electron contribution to the NII($N_2$; 3995.0 Å) current was found to be less than 0.05 percent over the 4 to 21 keV electron beam energy range.

By using the NII(NO; 3995.0 Å) line, which appears to be free of all spectral impurities, the full width at half maximum is found to be 1.6 Å in agreement with the assumed reciprocal linear dispersion of 16 Å/mm

31

and slit width of 100 $\mu$m. A slit width of 200 $\mu$m was used for the cross-section measurements since the observed intensity was proportional to the slit width and 200 $\mu$m was still sufficiently small to safely resolve the 5016.4-Å lines.

The current and pressure dependence was determined by measuring the radiative photon rate of each transition as a function of the beam current and chamber pressure, respectively. Figures 13 to 16 show the features of the current and pressure dependence of NII($N_2$; 5016.4 Å), NII(NO; 5016.4 Å), NII($N_2$; 3995.0 Å), and NII(NO; 3995.0 Å), respectively. The data were acquired at a beam energy of 10 keV and a slit width of 200 $\mu$m except for the pressure dependence of NII($N_2$; 3995.0 Å), which was obtained at 5 keV, and the NII(NO; 3995.0 Å) current dependence, which was obtained at 15 keV. In each case, the pressure was maintained at a constant value for the current dependence measurements, and the beam current was maintained at a constant value for the pressure dependence measurements.
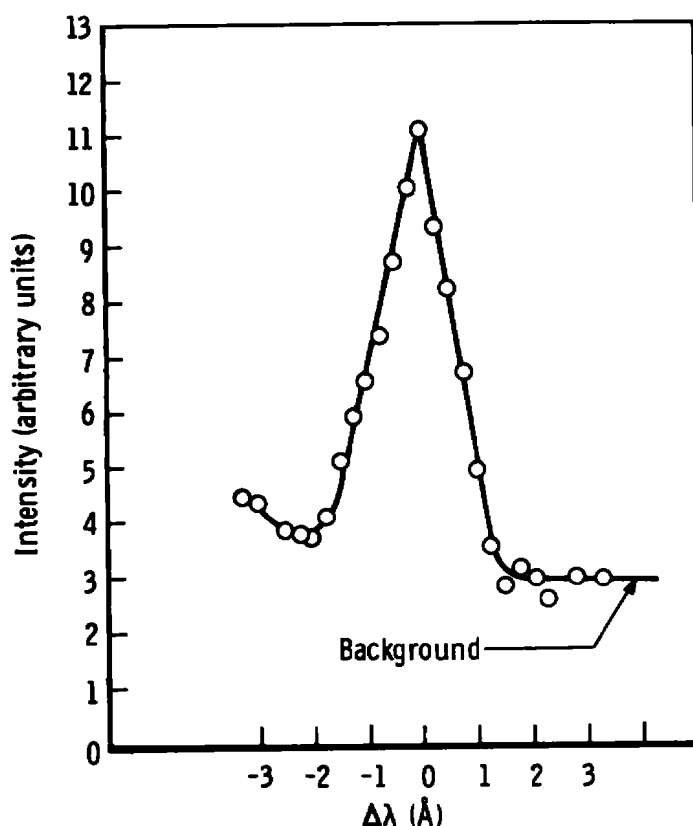


Figure 9. NII($N_2$; 5016.4 Å) line profile (slit width = 100 $\mu$m).
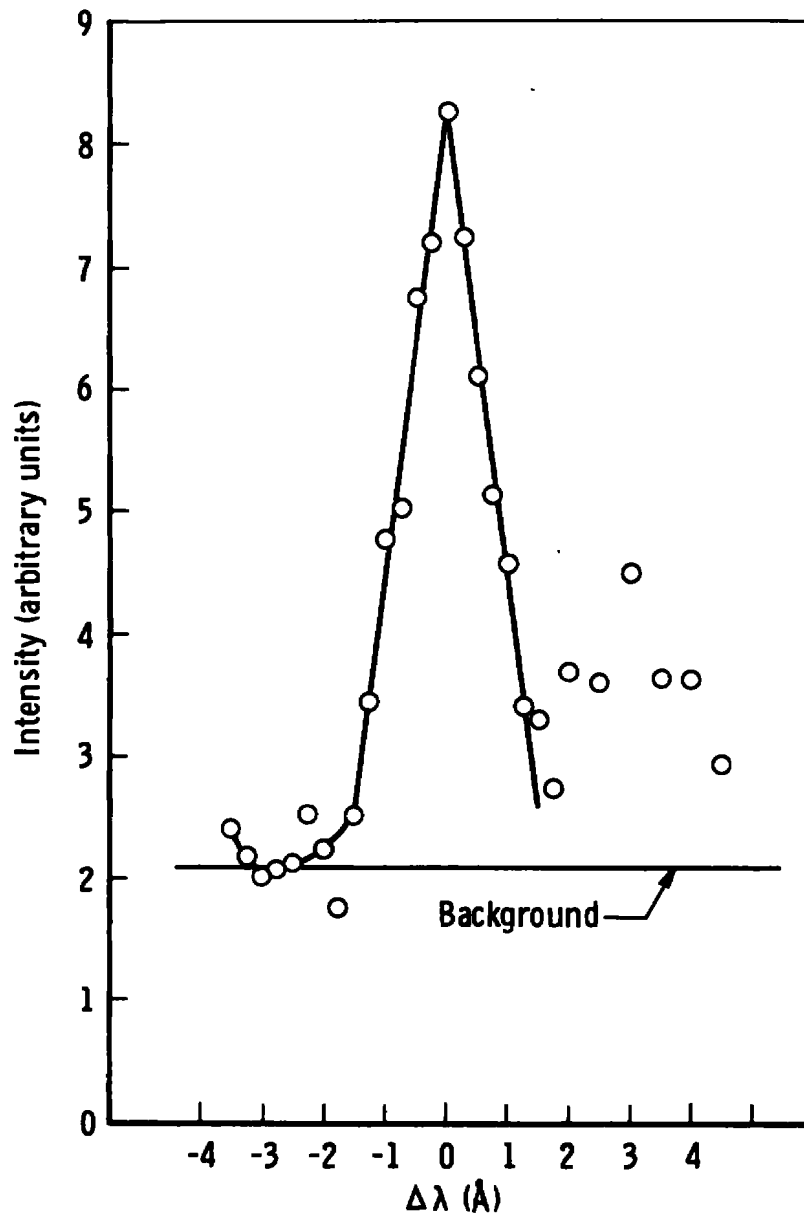
Figure 10. NII(NO; 5016.4 Å) line profile (slit width = 100 μm).
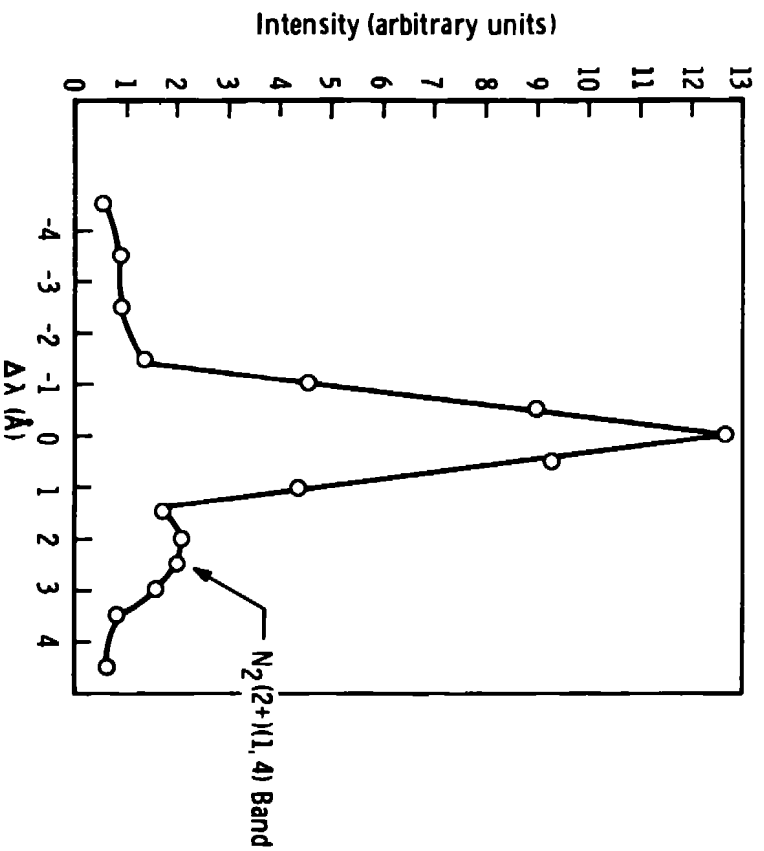
Figure 11. NII(N₂; 3995.0 Å) line profile (slit width = 100 μm).
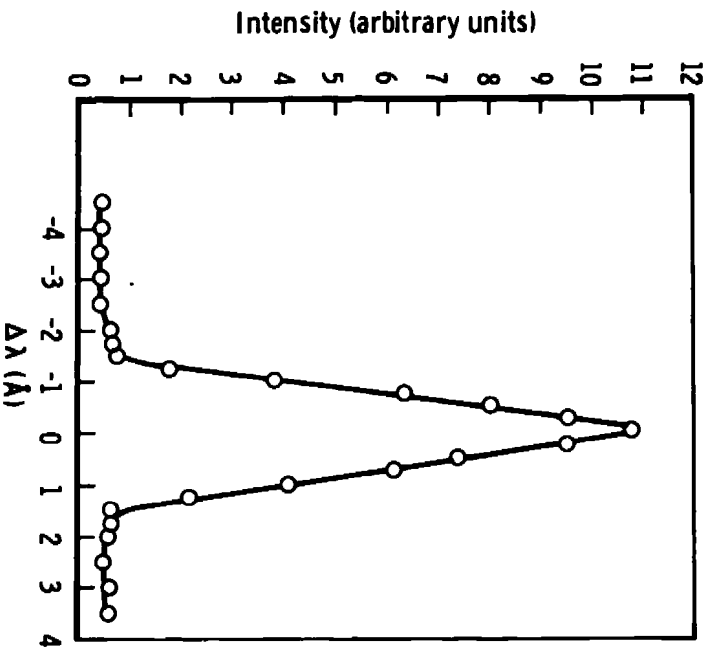
Figure 12. NII(NO; 3995.0 Å) line profile (slit width = 100 μm).
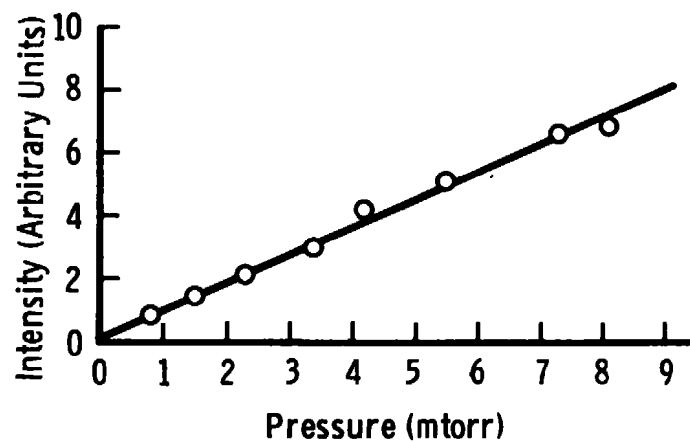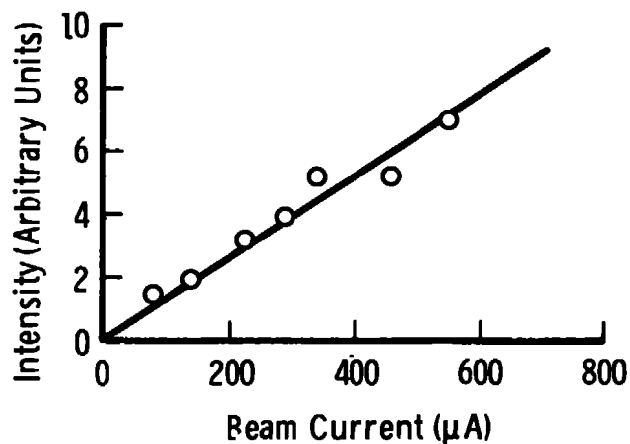
Figure 13. Current and pressure dependence of the molecular nitrogen NII($^3$F$^\circ$ → $^3$D) line at 5016.4 Å.
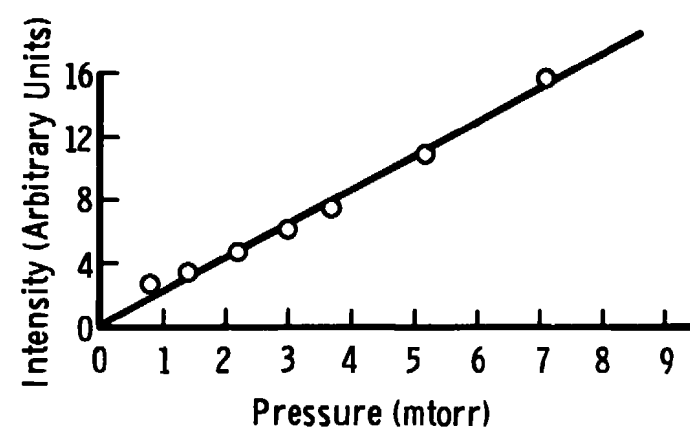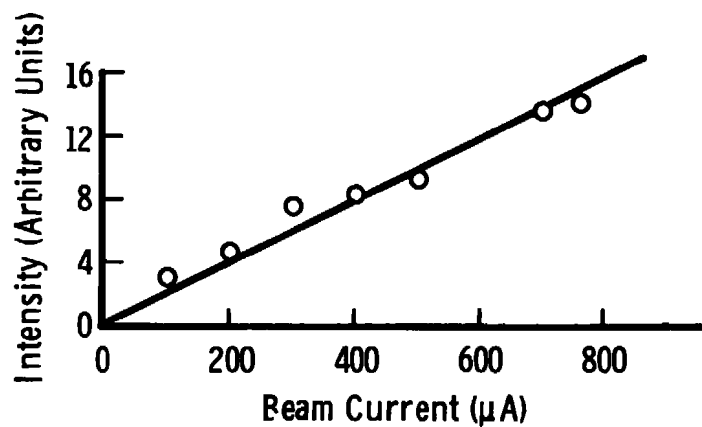


Figure 14. Current and pressure dependence of the nitric oxide NII($^3$F$^\circ$ → $^3$D) line at 5016.4 Å.
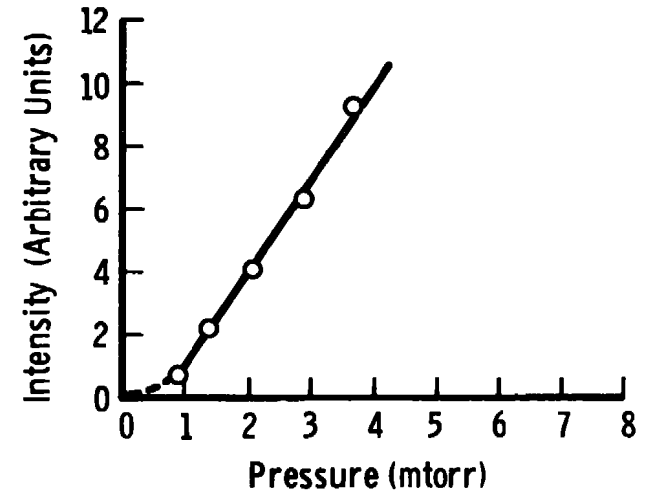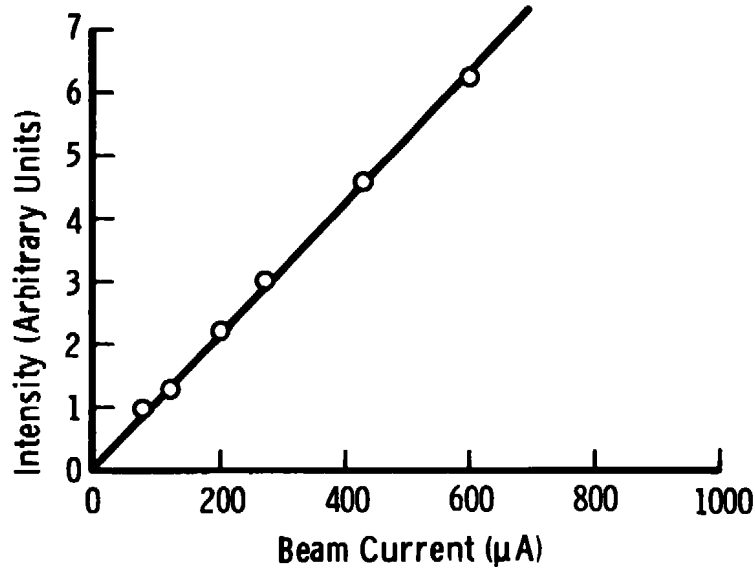
Figure 15.  Current and pressure dependence of the molecular
nitrogen NII($^1$D $\rightarrow$ $^1$P$^\circ$) line at 3995.0 Å.
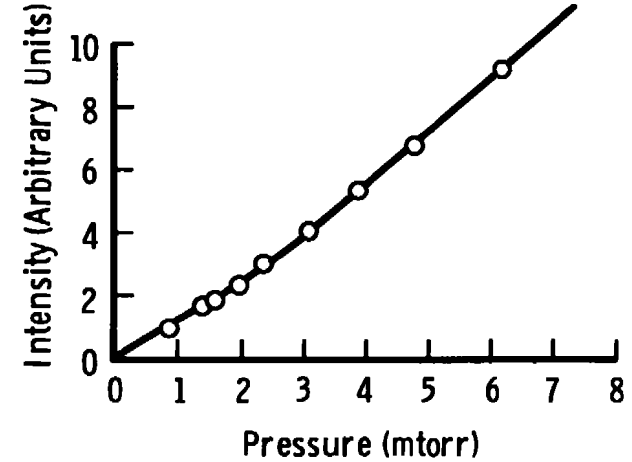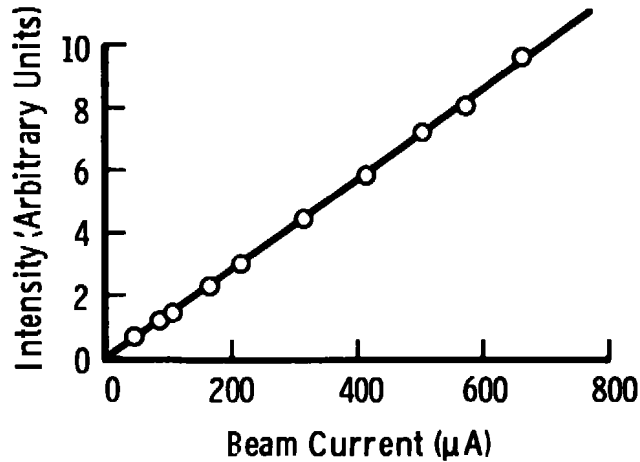
Figure 16.  Current and pressure dependence of the nitric
oxide NII($^1$D $\rightarrow$ $^1$P$^\circ$) line at 3995.0 Å.

The current and pressure dependences were obtained so that the cross-section measurements could be made at currents and pressures minimizing, or free of, secondary electron and collisional quenching effects and sufficiently linear to permit normalizing to the current and pressure. Figures 13 and 14 show the variations of the intensities for the two 5016.4-Å transitions with both current and pressure to be linear over the observed range and to pass through the origin, thus allowing the desired normalization. Similarly, Figs. 15 and 16 show a linear current dependence for both 3995.0-Å transitions over the observed range of beam current and the intensities extrapolate to zero for zero beam current. The pressure dependence of the NII($N_2$; 3995.0 Å) line is linear over the observed pressure range but does not pass through the origin, while the NII(NO; 2995.0 Å) line exhibits definite non-linearity at the lower pressures. In both cases, however, the linear region at high pressures can be extrapolated to an abscissa intercept of about 0.7 mtorr.

The energy dependence of the optical excitation cross sections was determined by measuring the radiative photon rate of each transition as a function of the electron beam energy. By using a spectrometer slit width of 200 $\mu$m, the total photon count summation at each wavelength of interest was accumulated over the time interval, less the photomultiplier tube dark count, was divided by the beam current, chamber pressure, and count interval time. The operating conditions were chosen such that the linearity of intensity with beam current and chamber pressure was ensured (Table 1).

**Table 1. Experimental Conditions during Data Acquisition**

| Specie | Energy Dependence | | Ratios at 10 keV | |
|---|---|---|---|---|
| | Beam Current ($\mu$A) | Pressure (mtorr) | Beam Current ($\mu$A) | Pressure (mtorr) |
| $N_2^+$ (1-) (0, 0) | $\leq$825 | $\leq$3.0 | 425 | 3.0 |
| NII ($N_2$; 5016.4 Å) | $\leq$800 | 10.2 | 425 | 8.7 |
| NII ($N_2$; 3995.0 Å) | $\leq$240 | 2.7 | 285 | 3.0 |
| NII (NO; 5016.4 Å) | $\leq$995 | 6.0 | 355 | 3.8 |
| NII (NO; 3995.0 Å) | $\leq$995 | 6.6 | 355 | 3.4 |

For the purpose of determining absolute values of the excitation cross section without the requirement of making absolute intensity measurements, it was decided that measurements of the strong, optically allowed $N_2^+(0,0)$ band of the $N_2^+$ First Negative System, $N_2^+(1-)$, would be performed and the results used for normalization of the NII results. This particular radiative system was selected because it has been verified that it obeys the prediction of the Bethe-Born relation for its energy dependence and absolute excitation cross sections are available for electron impact energies up to 6 keV (Ref. 13). Additionally, adequate theoretical and experimental knowledge exist for the collision-radiation process

$$N_2 X^1\Sigma_g^+(v = 0) + e^- \rightarrow N_2^+ B^2\Sigma_u^+(v = 0) + 2e^-$$

$$\rightarrow N_2^+ X^2\Sigma_g^+(v = 0) + h\nu$$

$$(56)$$
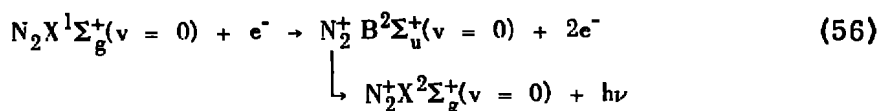
to enable accurate calculations of the intensity and profile of the $(0,0)$ band structure over a very wide energy range (Ref. 14). The energy dependence of the partial $N_2^+(1-)(0,0)$ band intensity was obtained by setting the spectrometer bandpass of 3.2 Å on the P branch peak and measuring the photon rate as a function of the electron energy. The data of Ref. 13 were used to obtain an extrapolated value of $9.93 \times 10^{-19}$ $cm^2$ for the $N_2^+(1-)(0,0)$ band absolute emission cross section at the electron beam energy of 10 keV, and the experimental results of the present study were normalized to this point. The results are shown in Fig. 17,
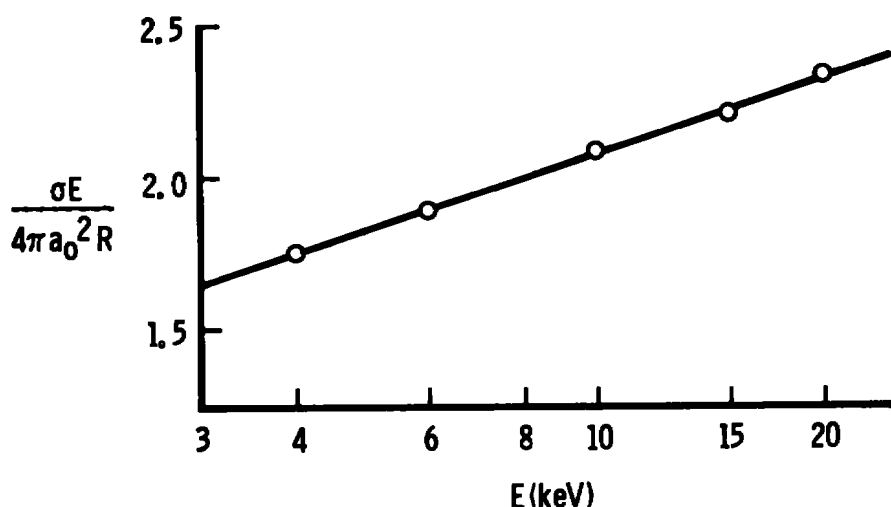


Figure 17. Bethe plot of the $N_2^+(1-)$ $(0,0)$ band optical excitation cross section.

and it is seen that the measured values of $\sigma E / 4\pi a_0^2 R$ are linear with $\ell n\ E$, verifying that the excitation of the $N_2^+(1-)(0,0)$ band is optically allowed over the energy range studied. These results are shown as well in Table 2. The slope obtained for the present results is $0.353 \pm 0.009$ with an intercept of $-1.18 \pm 0.08$ in agreement with a

Table 2. Energy Dependence of the $N_2^+(1-)$ (0,0) Band
Emission Cross Section

| E(keV) | $\dfrac{\sigma E}{4\pi a_0^2 R}$ | $\sigma\ (10^{-19}\ cm^2)$ |
|--------|-----------------|-------------|
| 4.0 | 1.75 | 20.9 |
| 6.0 | 1.88 | 15.0 |
| 10.0 | 2.08 | 9.96 |
| 15.0 | 2.21 | 7.05 |
| 20.0 | 2.33 | 5.58 |

slope of 0.35 given in Ref. 13. The standard deviation listed is the one-sigma value. Figures 18 and 19 show the current and pressure dependence measurements made at a beam energy of 10 keV and a slit width of 200 $\mu$m and the pressure dependence at 4 keV, respectively. In each case the observed radiative photon rate is linear and passes through the origin permitting the desired normalization to current and pressure.
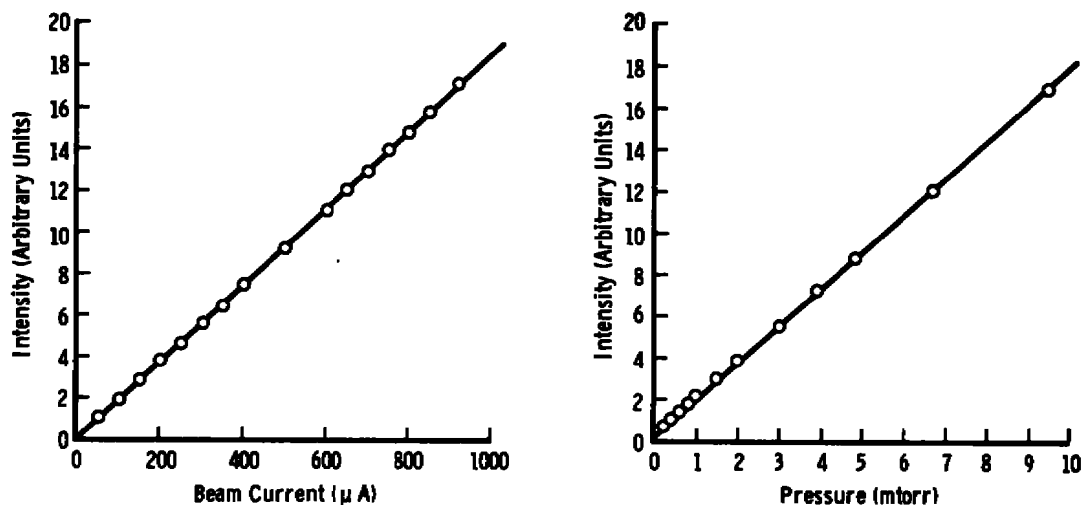


Figure 18. Current and pressure dependence of the $N_2^+(1-)$ (0,0) band.
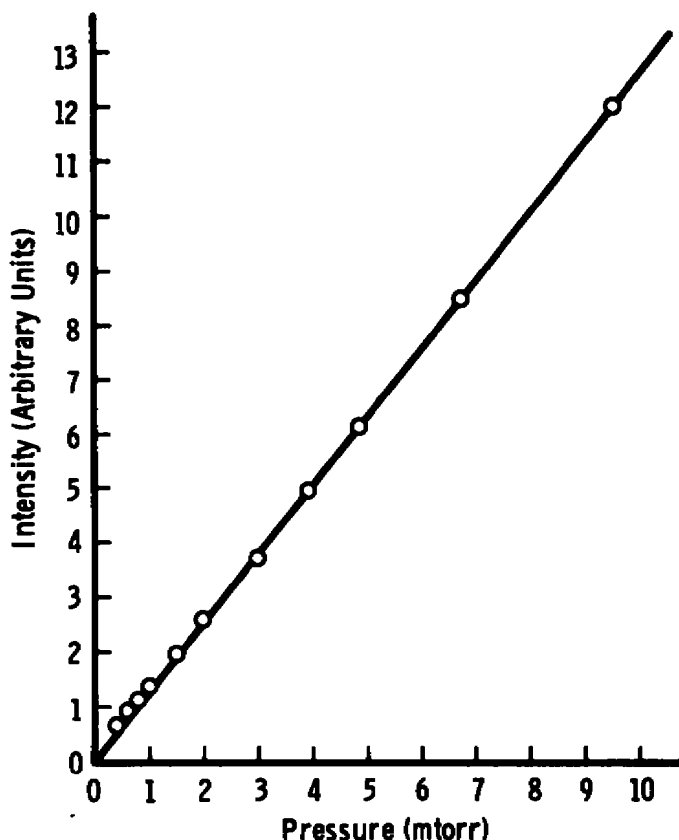
Figure 19. Pressure dependence of the $N_2^+(1-)$ (0,0) band at a beam energy of 4 keV.

To use the $N_2^+(1-)(0,0)$ band intensity for placing the NII data on an absolute scale, the entire band must be measured. The maximum slit width of the 0.5-m spectrometer used was 400 $\mu$m giving a bandpass of approximately 6.4 Å, which is less than approximately 1/4 that of the bandwidth. Consequently, it was necessary to adjust the measured partial band intensity to obtain the required total band intensity value.

The equations required for the theoretical calculation of the spectral intensity of a vibrational band in the $N_2^+(1-)$ system are given by Williams (Ref. 14). These equations enable the calculation of the theoretical relative intensity of each rotational line of the band as a function of the vibrational and rotational temperatures, assuming dipole rotational excitations and including nuclear spin considerations. The set of emission band strengths, excitation Franck-Condon factors, and other molecular parameters used in a computer calculation of the $N_2^+(1-)$ system rotational line intensities are listed or referenced in Ref. 5. The rotational line wavelength calculation, contained in the computer calculation, included

corrections for anharmonicity of the vibration and the influence of centrifugal stretching. The computer calculation then convolved the theoretical rotational line intensities with the spectrometer response function, using the reciprocal linear dispersion and spectrometer slit widths as input data, to calculate the theoretical spectrometer response from a given vibrational band of the $N_2^+(1-)$ system excited by an electron beam in 0.25-Å increments. The resulting plot of the $N_2^+(1-)(0,0)$ band at 280 K and 200 $\mu$m slit width is shown in Fig. 20 and may be compared with the experimentally obtained profile in Fig. 21. The theoretical ratio of the P branch peak at a slit width of 200 $\mu$m to the entire band was calculated to be 0.423. Variations of 0.25 Å in the spectrometer position near the P branch peak were shown by the calculation to change the partial band intensity by approximately 0.1 percent of the total band intensity.

The intensities of the $N_2^+(1-)(0,0)$ band and the NII lines were obtained using a slit width of 200 $\mu$m at an electron beam energy of 10 keV. The measured radiative photon count rates were corrected for photomultiplier tube dark count, and then divided by the beam current and chamber pressure. The results were corrected for background emission (5016.4-Å lines) and then divided by the relative spectral sensitivity factor $S(\lambda)$ to obtain relative intensity measurements. The background correction factors for the 5016.4-Å NII lines were obtained by subtracting the ratio of the background intensity and the total line intensity from unity. The relative intensity measurements for each spectral line were multiplied by the calculated partial to entire $N_2^+(1-)(0,0)$ band ratio and the $N_2^+(1-)(0,0)$ band absolute emission cross section to obtain the absolute optical excitation cross sections and subsequently the apparent cross sections. Table 3 shows the results of the measurements at the electron impact energy of 10 keV.

For the purpose of analyzing the numerous energy scans made for each transition, a computer program was developed and is shown in Table 4. The photon count rate, photomultiplier tube dark count, beam current, counting times for the intensity and dark count, and chamber pressure at each electron beam energy were used as input data. Also input was the normalized value of the ordinate at an electron beam energy of 10 keV, which is simply the absolute apparent cross section for the plot using the reciprocal beam energy as the abscissa and is equal to $\sigma E/4\pi a_0^2 R$ for the Bethe plot using $\ln E$ as the abscissa.
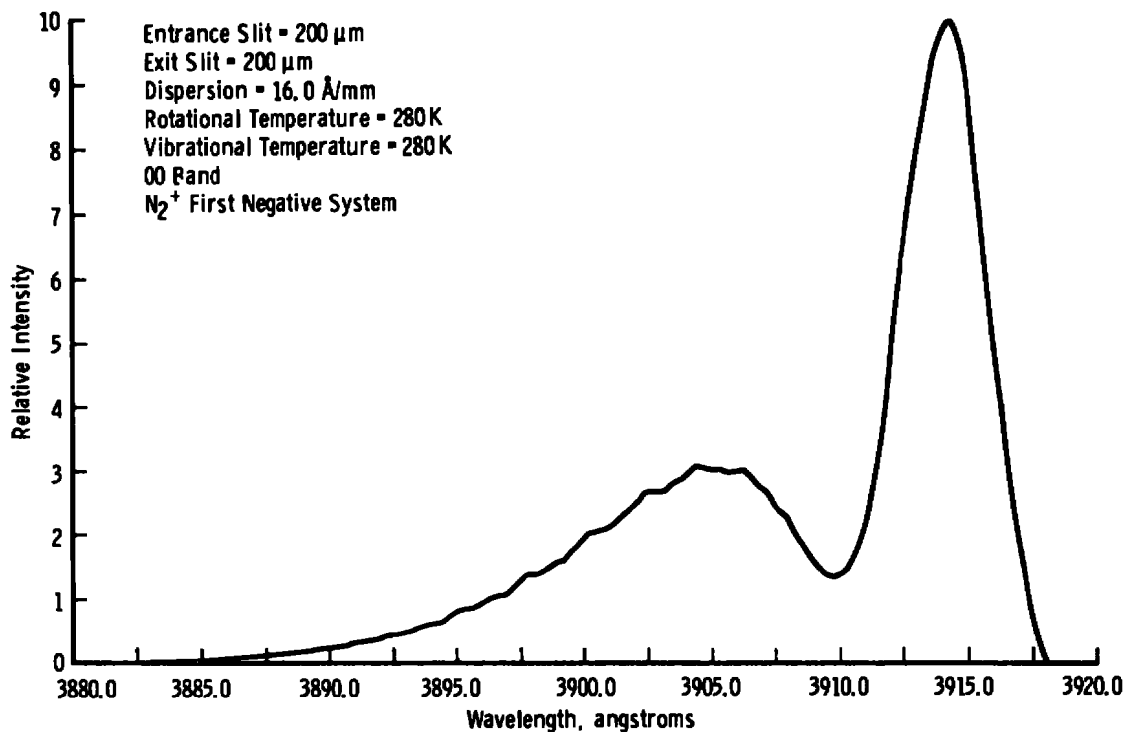
Figure 20.  Computer calculated $N_2^+$ (1-) (0,0) band profile.
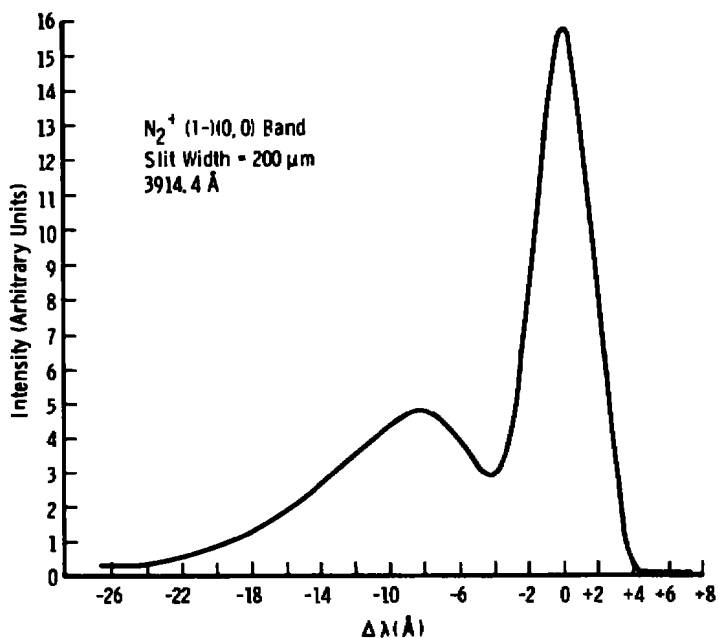


Figure 21.  $N_2^+$ (1-) (0,0) band profile (slit width = 200 μm).

Table 3. NII Apparent Cross Sections at 10 keV.

| Specie | $\lambda$, Å | Array | Multiplet | Background Correction Factor | $\dfrac{\sigma(\lambda)10^4}{\sigma(0,0)}$ | Optical* $\sigma(\lambda)$ $(10^{-22}\,cm^2)$ | $\beta_{u\ell}$ | Apparent $\sigma(\lambda)$ $(10^{-21}\,cm^2)$ | $\dfrac{\sigma E\,10^3}{4\pi a_0^2 R}$ |
|--------|------|-------|-----------|------|------|------|------|------|------|
| N$_2$ | 5016.4 | 2p3d→2p3p | $^3F^o$→$^3D$ | 0.735 | 2.25 | 2.23 | 0.155 | 1.44 | 3.01 |
|  | 3995.0 | 2p3p→2p3s | $^1D$→$^1p^o$ | 1 | 21.6 | 21.4 | 1 | 2.14 | 4.47 |
| NO | 5016.4 | 2p3d→2p3p | $^3F^o$→$^3D$ | 0.753 | 1.94 | 1.93 | 0.155 | 1.25 | 2.61 |
|  | 3995.0 | 2p3p→2p3s | $^1D$→$^1p^o$ | 1 | 17.7 | 17.6 | 1 | 1.76 | 3.68 |

*Normalized to the $N_2^+$(1-) (0,0) Band Emission Cross Section at 10 keV, 9.93 x $10^{-19}$ cm$^2$

## Table 4.  Program SUMDATA

```
         C          PROGRAM SUMDATA
0001            DIMENSION  BE(50),CR(30),BKG(30),BC(30),TCR(30),TBKG(30),
               1 P(30),IROW(400),ICOL(400),ICOUNT(20)
0002            DOUBLE PRECISION  SCR,DSCR,S(30),D(30),AVSD,WT(30),FOBE(50),
               1 SWI,SWIX,SWIXX,SWTY,SWTYY,SWTXY,SWWI,SWWTX,SWWTXX,DEN(20),
               2 SLP(20),CEP(20),SY(20),DSLP(20),DCEP(20),REFEU,RNORM(20),
               3 BETHE(50),DBETHE(50),BEX(20,20),BETHX(20,20),DBETHX(20,20),
               4 XBE(400),XBETH(400),XDBETH(400),A,CXBE(400),SUM,SSUM,
               5 ABETHE(50),ADBETH(50),DEM,SLM,CEM,SM,DSLM,DCEM
0003        400 FORMAT(10X,F10.0,6(5X,1PE12.5)/)
0004        401 FORMAT(5X,4(5X,1PE12.5)/)
0005        402 FORMAT (6X,2(1PE12.5))
0006        501 FORMAT (I3)
0007        502 FORMAT (6X,1PE12.5,I7)
0008        503 FORMAT (6X,F10.3,2F10.2,2F10.0,F10.3)
0009        504 FORMAT (20X,5(5X,1PE12.5),/)
0010        507 FORMAT (3I5)
0011        550 FORMAT (//,25X,9H SLOPE = ,1PE12.5,3X,18H WITH STD. DEV. = ,
               1 1PE12.5/)
0012        551 FORMAT(//,25X,13H INTERCEPT = ,1PE12.5, 3X,
               1    18H WITH STD. DEV. = ,1PE12.5)
0013        603 FORMAT(///,35X,16H** BETHE PLOT **,///)
0014        604 FORMAT(///,35X,28H** RECIPROCAL ENERGY PLOT **,////)
0015        605 FORMAT(//,25X,19HDATA NORMALIZED AT ,F7.0,3H EV,31H    USING AN OR
               1DINATE EQUAL TO ,1PE12.5,///)
0016        900 FORMAT (20A4)
0017        901 FORMAT (1H1,25X,20A4,//)
0018        902 FORMAT (//,25X,20A4,//)
0019        903 FORMAT (//,25X,20A4,//)
0020       1000 FORMAT (//,10X,'     ENERGY         ABSCISSA          ORDINATE
               1 STD. DEV.       WEIGHT          BETHE          STD. DEV.',/)
0021       1010 FORMAT (//,10X,'     SLOPES         STD. DEV.         INTERCEPTS
               1 STD. DEV. ',/)
0022       1020 FORMAT(//,28X,6HENERGY,10X,8HABSCISSA,9X,8HORDINATE,9X,
               1    9HSTD. DEV.,9X,6HWEIGHT,//)
0023            READ 900,A1,A2,A3,A4,A5,A6,A7,A8,A9,A10,A11,A12,A13,A14,A15,
               1A16,A17,A18,A20
0024            READ 900,B1,B2,B3,B4,B5,B6,B7,B8,B9,B10,B11,B12,B13,B14,B15,
               1B16,B17,B18,B19,B20
0025            READ 900,C1,C2,C3,C4,C5,C6,C7,C8,C9,C10,C11,C12,C13,C14,C15,
               1 C16,C17,C18,C19,C20
0026            READ 402,SIGMA0,E0
         C    SIGMA0 IS THE ABSOLUTE CROSS SECTION AT ENERGY E0 FOR A
         C    RECIPROCAL ENERGY PLOT
         C    SIGMA0 IS THE ORDINATE OF A BETHE PLOT AT ENERGY E0 WHEN JG=1
0027            JG = 1
0028            READ 507, ICMAX,IRMAX,NVAL
         C    IRMAX IS THE NUMBER OF ENERGY POINTS IN THE LARGEST DATA SET
         C    ICMAX IS THE NUMBER OF SETS OF DATA
         C    NVAL IS THE PRODUCT ICMAX*IRMAX AND DEFINES THE NUMBER OF
         C       ELEMENTS IN THE ARRAY
0029          5 READ 501,NK
         C    NK IS THE NUMBER OF SETS OF DATA, OR THE NUMBER OF SLOPES,
         C    WHICH WILL BE CALCULATED
0030            PRINT 901,A1,A2,A3,A4,A5,A6,A7,A8,A9,A10,A11,A12,A13,A14,A15,
               1A16,A17,A18,A19,A20
```

44

Table 4. Continued

```
0031            PKINT 902,B1,B2,B3,B4,B5,B6,B7,B8,B9,B10,B11,B12,B13,B14,B15,
                1B16,B17,B18,B19,B20
0032            PKINT 903,C1,C2,C3,C4,C5,C6,C7,C8,C9,C10,C11,C12,C13,C14,C15,
                1   C16,C17,C18,C19,C20
0033            IF(JG.EU.2)  GO TO 4
0034          3 PKINT 603
0035            GO TO 9
0036          4 PKINT 604
0037          9 CONTINUE
0038            DO 65  K=1,NK
0039         10 READ 501,NJ
        C       NJ IS THE NUMBER OF ENERGIES WHERE DATA WAS TAKEN TO OBTAIN A
        C       SET SUFFICIENT TO DETERMINE THE SLOPE
0040            DO 30 J=1,NJ
0041         15 READ 502,BE(J),NI
        C       BE IS THE BEAM ENERGY IN ELECTRON VOLTS
        C       NI IS THE NUMBER OF VALUES TAKEN AT EACH ENERGY
0042            DO 20 I=1,NI
0043         20 READ 503,BC(I),CR(I),BKG(I),TCR(I),TBKG(I),P(I)
        C       BC IS THE BEAM CURRENT IN UNITS OF 100 MICRO AMPS
        C       CR IS THE COUNT RATE IN PHOTONS PER SECOND
        C       BKG IS THE BACKGROUND COUNT RATE IN PHOTONS PER SECOND
        C       TCR IS THE SIGNAL COUNTING TIME IN SECONDS
        C       TBKG IS THE BACKGROUND CO UTING TIME IN SECONDS (DARK COUNT)
        C       P IS THE PRESSURE IN MILLITORR
        C       CALCULATION OF AVERAGE INTENSITY AND STANDARD DEVIATION AT
        C       EACH ENERGY
0044            SCR=0.0
0045            DSCR=0.0
0046            DO 25 I=1,NI
0047            SCR=SCR+(CR(I)-BKG(I))/(BC(I)*P(I))
0048         25 DSCR=DSCR+(CR(I)/TCR(I)+BKG(I)/TBKG(I))/(BC(I)*BC(I)*P(I)*P(I))
0049            S(J)=SCR/NI
        C       S(J) IS THE AVERAGE C UNT RATE AT THE ENERGY CORRESPONING TO J
0050            D(J)=DSQRT(DSCR)/NI
        C       D(J) IS THE STAND AD DEVIATION ASSOCIATED WITH S(J)
        C       CALCULATION OF THE STATISTICAL WEIGHTS
0051            IF(JG. EU.2)  GO TO 36
0052         26 S(J)=S(J)*BE(J)
        C       S(J) IS THE P RDUCT OF THE AVERAGE COUNT RATE AND THE
        C       ENERGY CORRESPONDING TO J
0053            D(J)=D(J)*BE(J)
0054         30 CONTINUE
0055            KT = 2
0056            IF(KT.EU.1)  GO TO 36
0057         31 AVSD=0.0
0058            DO 32 J=1,NJ
0059         32 AVSD=AVSD+D(J)
0060            AVSD=AVSD/NJ
        C       AVSD IS USED TO CALCULATE THE WEIGHTS AND IS THE AVERAGE OF
        C       THE STANDARD DEVIATIONS FOR THIS SET OF DATA
0061            DO 35 J=1,NJ
0062         35 WT(J)=(AVSD/D(J))**2
0063            GO TO 40
0064         36 DO 37  J=1,NJ
0065         37 WT(J) = 1.0
```

## Table 4. Continued

```
          C      WT(J) IS  TE STATISTICAL WEIGHT ASSOCIATED WITH S(J)
 0066     40 CONTINUE
          C      CALCULATION OF ABSCISSA VALUES
 0067        DO 55 J=1,NJ
 0068          IF(JG.EU.1)  GO TO 50
 0069          IF(JG.EU.2)  GO TO 51
 0070     50 FOBE(J)=ALOG (BE(J))
 0071        GO TO 55
 0072     51 FOBE(J)=1.0/BE(J)
 0073     55 CONTINUE
          C      FOBE(J) IS THE ABSCISSA USED FOR THESE SETS OF DATA
          C      WEIGHTED LEAST SQUARES FIT
          C      CALCULATION OF SLOPE AND INTERCEPT AND RESPECTIVE STANDARD
          C        DEVIATIONS
 0074        SWT=0.0
 0075        SWTX=0.0
 0076        SWTXX=0.0
 0077        SWTY=0.0
 0078        SWTYY=0.0
 0079        SWTAY=0.0
 0080        SWWT=0.0
 0081        SWWTX=0.0
 0082        SWWTXX=0.0
 0083        DO 60 J=1,NJ
 0084        SWT=SWT+WT(J)
 0085        SWTX=SWTX+WT(J)*FOBE(J)
 0086        SWTXX=SWTXX+WT(J)*FOBE(J)*FOBE(J)
 0087        SWTY=SWTY+WT(J)*S(J)
 0088        SWTYY=SWTYY+WT(J)*S(J)*S(J)
 0089        SWTXY=SWTAY+WT(J)*S(J)*FOBE(J)
 0090        SWWT=SWWT+WT(J)*WT(J)
 0091        SWWTX=SWWTX+WT(J)*WT(J)*FOBE(J)
 0092     60 SWWTXX=SWWTXX+WT(J)*WT(J)*FOBE(J)*FOBE(J)
 0093        DEN(K)=SWT*SWTXX-SWTX*SWTX
 0094        SLP(K)=(SWT*SWTXY-SWTX*SWTY)/DEN(K)
          C      SLP(K) IS THE SLOPE OF THE DATA SET K
 0095        CEP(K)=(SWTY*SWTXX-SWTX*SWTXY)/DEN(K)
          C      CEP(K) IS THE INTERCEPT OF THE DATA SET K
          C      CALCULATION OF STANDARD DEVIATION FOR SLOPE
 0096        SY(K)=DSQRT((SWTYY-(SWTY*SWTY*SWTXX-2.0*SWTXY*SWTX*SWTY
 1     +SWT*SWTXY*SWTAY)/DEN(K))/(NJ-2))
 0097        USLP(K)=SY(K)*DSQRT(SWT*SWT*SWWTXX+SWTX*SWTX*SWWT
 1     -2.0*SWT*SWTX*SWWTX)/DEN(K)
          C      DSLP(K) IS THE STANDARD DEVIATION ASSOCIATED WITH SLP(K)
 0098        DCEP(K)=SY(K)*DSQRT(SWTX*SWTX*SWWTXX+SWTXX*SWTXX*SWWT-2.0*
 1     SWTX*SWTXX*SWWTX)/DEN(K)
          C      DCEP(K) IS THE STANDARD DEVIATION ASSOCIATED WITH CEP(K)
 0099        IF(JG.EU.1)   GO TO 92
 0100     91 REFEO=1.0/EO
 0101        GO TO 93
 0102     92 CONTINUE
 0103        REFEO=ALOG (EO)
 0104     93 RNORM(K) = SIGMAO/(SLP(K)*REFEO+CEP(K))
 0105        DO 94  J=1,NJ
 0106        BETHE(J) = RNORM(K) * S(J)
 0107     94 DBETHE(J)=BETHE(J)*DSQRT(((DSLP(K)*DSLP(K)* REFEO  *  REFEO  +DCE
```

## Table 4. Continued

```
                    IP(K)*UCEP(K))*RNORM(K)*RNORM(K)/((SLP(K)*  REFEO  +CEP(K))**2))+D(
                    2J)*D(J)/(S(J)*S(J)))
            C       BETHE(J) IS THE ABSOLUTE EXCITATION CROSS SECTION FOR A
            C          RECIPROCAL ENERGY PLOT
            C       BETHE(J) IS THE ORDINATE OF A BETHE PLOT WHEN JG=1 AND
            C          IS EQUAL TO SIGMA*E/(4*PI*A*A*R)
            C       RNORM IS A CONSTANT WHICH PUTS THE DATA ON AN ABSOLUTE SCALE BASED
            C          ON THE ORDINATE SIGMAO AT ENERGY EO
            C       DBETHE IS THE STANDARD DEVIATION ASSOCIATED WITH THE VALUE
            C          OF BETHE(J)
0108            199 PRINT 1000
0109                DO 200 J=1,NJ
0110            200 PRINT 400,BE(J),FDBE(J),S(J),D(J),WT(J),BETHE(J),DBETHE(J)
            C       IF NJ < IRMAX, THE REMAINING VALUES OF  BE, BETHE, AND DBETHE ARE
            C          SET EQUAL TO ZERO
0111                IRMAX2 = IRMAX + 1
0112                JO = NJ + 1
0113                DO 16   J = JO,IRMAX2
0114                BE(J) = 0.0
0115                BETHE(J) = 0.0
0116             16 DBETHE(J) = 0.0
            C       NOW WE CHANGE NOTATION TO UTILIZE A TWO DIMENSIONAL ARRAY
0117                DO 17  J = 1,IRMAX
0118                BEX(J,K) = BE(J)
0119                BETHX(J,K) = BETHE(J)
0120             17 DBETHX(J,K) = DBETHE(J)
0121             65 CONTINUE
0122                PRINT 1010
0123                DO 201  K=1,NK
0124            201 PRINT 401,SLP(K),DSLP(K),CEP(K),UCEP(K)
0125                PRINT 605,E0,SIGMAO
0126            206 PRINT 1010
0127                DO 202  K=1,NK
0128                SLP(K)=RNORM(K)*SLP(K)
0129                DSLP(K)=RNORM(K)*DSLP(K)
0130                CEP(K)=RNORM(K)*CEP(K)
0131                UCEP(K)=RNORM(K)*UCEP(K)
0132            202 PRINT 401,SLP(K),DSLP(K),CEP(K),UCEP(K)
0133            205 CONTINUE
            C       CHANGE ENERGY MATRIX TO VECTOR AND SAVE ARRAY POSITION
0134                JK = 1
0135                DO 301   J = 1,IRMAX
0136                DO 301   K = 1,ICMAX
0137                XBE(JK) = BEX(J,K)
0138                XBETH(JK)  = BETHX(J,K)
0139                XDBETH(JK) = DBETHX(J,K)
0140                IROW(JK) = J
0141                ICOL(JK) = K
0142                JK = JK + 1
0143            301 CONTINUE
            C       XBE(JK)  IS THE ENERGY MATRIX IN VECTOR FORM
            C       XBETH(JK) IS THE ORDINATE MATRIX IN VECTOR FORM
            C       XDBETH(JK) IS THE STD. DEV. MATRIX IN VECTOR FORM
            C       IROW(JK) IS THE ROW POSITION VALUE
            C       ICOL(JK) IS THE COLUMN POSITION VALUE
            C       NOW ARRANGE ARRAY FROM SMALL TO LARGE
```

47

**Table 4. Continued**

```
C          BEAM ENERGIES ARE ORDERED SUCH THAT XBE GIVES THE BEAM
C          ENERGY AT COORDINATES IROW AND ICOL WHERE ICOL CORRESPONDS
C          TO THE ORIGINAL DATA SET NUMBER AND IROW CORRESPONDS TO THE
C          ENERGY DATA POINTS IN THAT SET
C          NVAL IS THE NUMBER OF VALUES IN THE ARRAY
0144       NVAL2 = NVAL - 1
0145       DO 302  JK = 1,NVAL2
0146       JJ = JK + 1
0147       DO 303   K = JJ,NVAL
0148       IF (XBE(JK).LE.XBE(K))  GO TO 303
0149       A = XBE(K)
0150       XBE(K)=XBE(JK)
0151       XBE(JK)=A
0152       A = XBETH(K)
0153       XBETH(K) = XBETH(JK)
0154       XBETH(JK) = A
0155       A = XDBETH(K)
0156       XDBETH(K) = XDBETH(JK)
0157       XDBETH(JK) = A
0158       I=IROW(K)
0159       IROW(K)=IROW(JK)
0160       IROW(JK)=I
0161       I=ICOL(K)
0162       ICOL(K)=ICOL(JK)
0163       ICOL(JK)=I
0164   303 CONTINUE
0165   302 CONTINUE
C          NOW COUNT NUMBER OF LIKE ENERGIES
0166       N = 0
C          N COUNTS LIKE VALUES OF BEAM ENERGY, XBE
0167       DO 304  JK = 1,NVAL
0168       IF (JK.EQ.1) GO TO 320
0169       IF (XBE(JK).EQ.CXBE(N)) GO TO 304
C          IF XBE(J) EQUALS CXBE(N), IT HAS ALREADY BEEN COUNTED
0170   320 N = N + 1
0171       CXBE(N) = XBE(JK)
0172       ICOUNT(N) = 1
C          ICOUNT IS THE NUMBER OF TIMES EACH ENERGY, CXBE, APPEARS
0173       K = JK + 1
0174       DO 305  L = K,NVAL
0175       IF (CXBE(N).NE.XBE(L)) GO TO 349
0176       ICOUNT(N) = ICOUNT(N) + 1
0177   305 CONTINUE
0178   349 CONTINUE
0179   304 CONTINUE
0180       ZERO = 0.0
0181       LX = 1
0182       IF (CXBE(LX).NE.ZERO) GO TO 291
0183       I = ICOUNT(1) + 1
0184       DO 292  JKK = I,NVAL
0185       JK = JKK - I + 1
0186       XBETH(JK) = XBETH(JKK)
0187   292 XDBETH(JK) = XDBETH(JKK)
0188       NVAL = NVAL - I + 1
0189       DO 290  KK = 2,N
0190       L = KK - 1
```

## Table 4. Continued

```
0191              ICOUNT(L) = ICOUNT(KK)
0192         290  CXBE(L) = CXBE(KK)
0193              N = N - 1
0194         291  CONTINUE
        C             NOW AVERAGE BETHE AND COMBINE STANDARD DEVIATIONS AT
        C             EACH ENERGY
0195              JJ = 1
0196              DO 306  L = 1,N
0197              LL = ICOUNT(L) + JJ - 1
0198              SUM = 0.0
0199              SSUM = 0.0
0200              DO 307  JK = JJ,LL
0201              SUM = SUM + XBETH(JK)
0202              SSUM = SSUM + XDBETH(JK)*XDBETH(JK)
0203         307  CONTINUE
0204              ABETHE(L) = SUM/ICOUNT(L)
0205              ADBETH(L) =DSQRT(SSUM)/ICOUNT(L)
0206              JJ = LL + 1
0207         306  CONTINUE
        C     ABETHE IS THE AVERAGE ORDINATE WITH STANDARD DEVIATION ADBETHE
        C         FOR EACH DISCRETE BEAM ENERGY CXBE
        C         WEIGHTED LEAST SQUARES FIT
        C     CALCULATION OF ABSCISSA VALUES
0208              DO 309  L=1,N
0209              BE(L)=CXBE(L)
0210              S(L)=ABETHE(L)
0211         309  D(L)=ADBETH (L)
0212              IF(JG.EQ.2)  GO TO 312
0213              PRINT 603
0214         312  CONTINUE
0215              PRINT 604
0216              DO 316  L=1,N
0217              IF(JG.EQ.1)  GO TO 315
0218         310  FOBE(L)=1.0/BE(L)
0219              GO TO 316
0220         315  FOBE(L)=ALOG (BE(L))
0221         316  CONTINUE
0222              IF (JG.NE.3)  GO TO 313
0223              PRINT 603
0224         313  CONTINUE
        C         AVSD IS USED IN THE WEIGHT CALCULATION AND IS THE AVERAGE
        C         OF THE STANDARD DEVIATIONS FOR THIS SET OF DATA
0225              AVSD=0.0
0226              DO 308  L=1,N
0227         308  AVSD = AVSD + D(L)
0228              AVSD=AVSD/N
0229              DO 311  L=1,N
0230         311  WT(L) = (AVSD/D(L))**2
0231              PRINT 1020
0232              DO 351  L = 1,N
0233         351  PRINT 504,BE(L),FOBE(L),S(L),D(L),WT(L)
        C     CALCULATION OF SLOPE AND INTERCEPT AND RESPECTIVE STANDARD
        C         DEVIATIONS
0234              SWT=0.0
0235              SWTX=0.0
0236              SWTXX=0.0
```

49

## Table 4. Concluded

```
0237                    SWTY=0.0
0238                    SWTYY=0.0
0239                    SWTXY=0.0
0240                    SWWT=0.0
0241                    SWWTX=0.0
0242                    SWWTXX=0.0
0243                    DO 350  L=1,N
0244                    SWT=SWT+WT(L)
0245                    SWTX=SWTX+WT(L)*FOBE(L)
0246                    SWTXX=SWTXX+WT(L)*FOBE(L)*FOBE(L)
0247                    SWTY=SWTY+WT(L)*S(L)
0248                    SWTYY=SWTYY+WT(L)*S(L)*S(L)
0249                    SWTXY=SWTXY+WT(L)*S(L)*FOBE(L)
0250                    SWWT=SWWT+WT(L)*WT(L)
0251                    SWWTX=SWWTX+WT(L)*WT(L)*FOBE(L)
0252           350      SWWTXX=SWWTXX+WT(L)*WT(L)*FOBE(L)*FOBE(L)
0253                    DEM=SWT*SWTXX-SWTX*SWTX
0254                    SLM=(SWT*SWTXY-SWTX*SWTY)/DEM
               C        SLM IS THE SLOPE OF THE  DATA
0255                    CEM=(SWTY*SWTXX-SWTX*SWTXY)/DEM
               C        CEM IS THE INTERCEPT IF THE DATA
0256                    SM=DSQRT((SWTYY-(SWTY*SWTY*SWTXX-2.0*SWTXY*SWTX*SWTY
               1        +SWT*SWTXY*SWTXY)/DEM)/(N-2))
0257                    DSLM=SM*DSQRT(SWT*SWT*SWWTXX+SWTX*SWTX*SWWT
               1        -2.0*SWT*SWTX*SWWTX)/DEM
               C        DSLM IS THE STANDARD DEVIATION ASSOCIATED WITH SLM
0258                    DCEM=SM*DSQRT(SWTX*SWTX*SWWTXX+SWTXX*SWTXX*SWWT-2.0*
               1        SWTX*SWTXX*SWWTX)/DEM
               C        DCEM IS THE STANDARD DEVIATION ASSOCIATED WITH CEM
0259                    PRINT 550, SLM,DSLM
0260                    PRINT 551, CEM,DCEM
0261                    IF(JG.EQ.1)  GO TO 353
0262                    IF(JG.GT.2)  GO TO 353
0263                    CONST = 4.788 E-15
               C        CONST IS EQUAL TO 4*PI*A*A*R IN UNITS OF EV*CM*CM, WHERE
               C           A IS THE FIRST BOHR RADIUS AND R IS THE RYDBERG ENERGY
0264                    DO 354   L = 1,N
0265                    FOBE(L) = ALOG(BE(L))
0266                    S(L) = S(L)*BE(L)/CONST
0267           354      D(L) = D(L)*BE(L)/CONST
0268                    JG = JG + 1
0269                    GO TO 316
0270           353      STOP
0271                    END
```

By following the derivation of Beers (Ref. 15) for a least-squares fit and noting the derivation of Bacon (Ref. 16) for the weighted slope and intercept, equations for the weighted standard deviations of the weighted slope and intercept were derived, the details of which are listed in the appendix of Ref. 17. Beginning with the standard deviation of a random count as the square root of the count, the computer calculation computes the statistical weight associated with each energy and performs the weighted least-squares fit for each energy scan. The coordinates are $\sigma$ versus $E^{-1}$ or $\sigma E / 4\pi a_0^2 R$ versus $\ell n\ E$ as desired. Next, a normalization constant is computed such that the straight line determined by the weighted least-squares fit passes through the ordinate value used as input data at 10 keV, and the observed intensity measurements determined as a function of electron beam energy are put on an absolute scale by multiplying each value by this normalization constant. After each set of data is thus scaled to give absolute apparent cross sections, or $\sigma E / 4\pi a_0^2 R$ for a Bethe plot, the data are sorted to give all cross-section values, or $\sigma E / 4\pi a_0^2 R$ for a Bethe plot, and their respective standard deviations occurring at each electron beam energy. After averaging the ordinate values, a weighted least-squares fit is performed, and the ordinate and abscissa values as well as the slope and intercept are printed along with their respective standard deviations and statistical weights. Thus, the observed intensity measurements for each spectral line determined as a function of electron beam energy were used with the 10-keV data of the NII lines and the $N_2^+(1-)(0, 0)$ band to obtain absolute values of the apparent cross sections. The values thus obtained for the apparent cross sections of the NII $^3F^\circ$ and NII $^1D$ states produced by dissociative excitation of $N_2$ and NO are listed in Tables 5 and 6, respectively.

The partial Grotrian diagram shown in Fig. 22 indicates qualitatively the possible cascade contributions to the NII $^3F^\circ$ and NII $^1D$ levels (Ref. 18). The possible existence of these transitions induced by electron beam excitation is at present unknown, and thus no cascade corrections, if they do indeed exist, can be made on the present cross-section values.

The apparent cross sections of the NII $^1D$ level produced by dissociative excitation of $N_2$ and NO result directly from the optical cross-section measurements since the NII $^1D$ level radiates by only the observed transition (Fig. 22). The NII $^1F^\circ$ level, however, has three competing radiative transitions (Fig. 22), and the optical cross section at 10 keV was divided by the branching factor of 0.155 as determined from Ref. 18 in order to obtain the apparent cross section. Consequently, the apparent cross sections possess the accuracy of the life time calculations of Ref. 18. Since the life time is the same for the NI $^3F^\circ$ level, regardless of molecular

Table 5. Energy Dependence of the NII($^3$F°) Apparent Cross Section

| N$_2$ | | | NO | | |
|---|---|---|---|---|---|
| E (keV) | $\sigma(10^{-21}$ cm$^2)$ | $\dfrac{\sigma E\,10^3}{4\pi a_0^2 R}$ | E (keV) | $\sigma(10^{-21}$ cm$^2)$ | $\dfrac{\sigma E\,10^3}{4\pi a_0^2 R}$ |
| 4.0 | 3.6 | 3.0 | 4.0 | 2.8 | 2.3 |
| 5.0 | 2.8 | 2.9 | 5.0 | 2.3 | 2.4 |
| 6.0 | 2.4 | 3.0 | 6.0 | 1.9 | 2.4 |
| 7.0 | 2.0 | 3.0 | 7.0 | 1.7 | 2.5 |
| 8.0 | 1.8 | 3.0 | 8.0 | 1.5 | 2.6 |
| 10.0 | 1.5 | 3.0 | 10.0 | 1.3 | 2.7 |
| 12.0 | 1.2 | 3.0 | 12.0 | 1.1 | 2.7 |
| 15.0 | 0.92 | 2.9 | 15.0 | 0.89 | 2.8 |
| 18.0 | 0.89 | 3.4 | 18.0 | 0.75 | 2.8 |
| 20.0 | 0.89 | 3.7 | 20.0 | 0.68 | 2.8 |

Table 6. Energy Dependence of the NII($^1$D) Apparent Cross Section

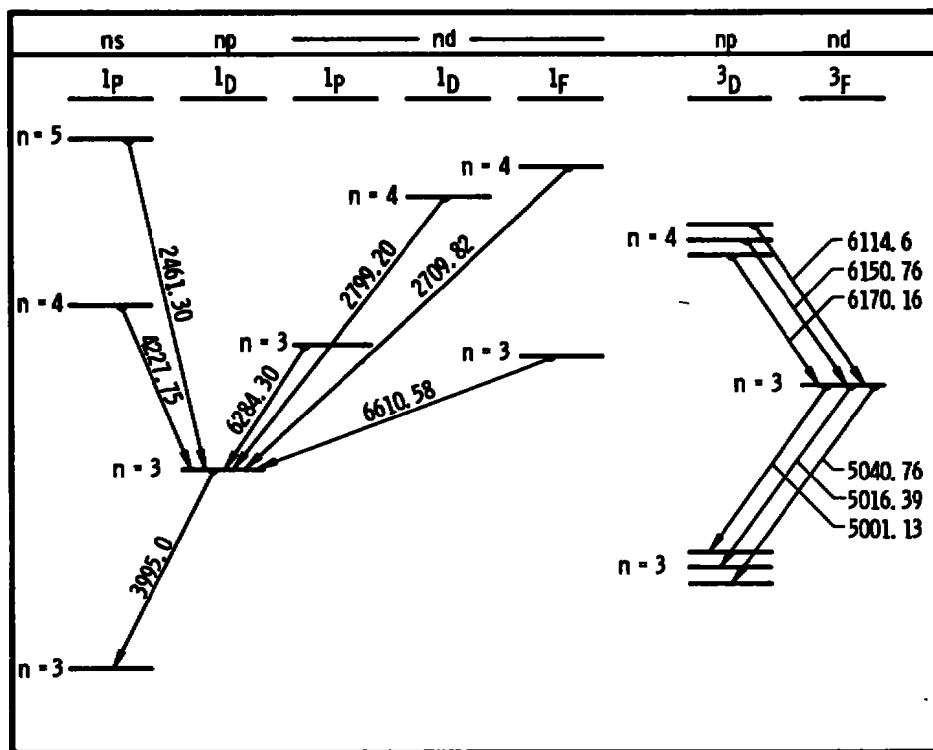| N$_2$ | | | NO | | |
|---|---|---|---|---|---|
| E (keV) | $\sigma(10^{-21}$ cm$^2)$ | $\dfrac{\sigma E\,10^3}{4\pi a_0^2 R}$ | E (keV) | $\sigma(10^{-21}$ cm$^2)$ | $\dfrac{\sigma E\,10^3}{4\pi a_0^2 R}$ |
| 4.0 | 5.2 | 4.4 | 4.0 | 3.4 | 2.8 |
| 4.5 | 3.9 | 3.6 | 5.0 | 3.1 | 3.2 |
| 5.0 | 4.3 | 4.5 | 6.0 | 2.8 | 3.5 |
| 6.0 | 3.3 | 4.2 | 7.0 | 2.5 | 3.6 |
| 7.0 | 3.0 | 4.3 | 8.0 | 2.2 | 3.7 |
| 8.0 | 2.6 | 4.3 | 10.0 | 1.8 | 3.7 |
| 10.0 | 2.1 | 4.5 | 12.0 | 1.5 | 3.7 |
| 12.0 | 1.8 | 4.6 | 15.0 | 1.2 | 3.7 |
| 15.0 | 1.5 | 4.7 | 17.0 | 1.1 | 3.7 |
| 18.0 | 1.3 | 4.7 | 18.0 | 0.95 | 3.6 |
| 20.0 | 1.2 | 5.0 | 19.0 | 0.89 | 3.5 |
| 21.0 | 1.1 | 4.8 | 20.0 | 0.84 | 3.5 |
| | | | 21.0 | 0.78 | 3.4 |

Figure 22. Partial Grotrian diagram for NII.

specie involved, the ratio of the NII($N_2$; 5016.4 Å) optical cross section and the NII(NO; 5016.4 Å) optical cross section is identical to that of the apparent cross-section ratio, and the dependence on the accuracy of the life time calculation is eliminated. The ratios thus obtained are

$$\sigma[NII(N_2;5016.4\text{ Å})]/\sigma[NII(NO; 5016.4\text{ Å})] = 1.16$$

and

$$\sigma[NII(N_2; 3995.0\text{ Å})]/\sigma[NII(NO; 3995.0\text{ Å})] = 1.22$$

determined at an electron beam energy of 10 keV.

By using the Bethe-Born analysis of Section 1.2, the values of several parameters can be derived. For optically allowed transitions, the slope of a Bethe plot is equal to the dipole-matrix-element squared, $M_n^2$, for the transition; the constant $\ln C_n$ is equal to the ratio of the intercept to the slope; the constant, $\overline{K}a_o$, is derived from the value of $C_n$ using Eq. (30); and the optical oscillator strength, $f_n$, is defined by Eq. (12). First-order forbidden transitions yield the constant $b_n$ by dividing the slope of a reciprocal energy plot by $4\pi a_o^2 R$ which is equivalent to using the expression $b_n = \sigma E/4\pi a_o^2 R$. For the $N_2^+(1-)(0,0)$, the

following parameters were calculated:

$$M_n^2 = 0.353 \pm 0.009$$

$$C_n = 0.035 \pm 0.009$$

$$\bar{K}a_o = 0.110 \pm 0.001$$

and

$$f_n = 0.49 \pm 0.01$$

## 4.0 DISCUSSION AND CONCLUSIONS

The dependence of the $N_2^+(1-)(0,0)$ band emission cross section on the energy of the incident electrons was in excellent agreement with the results of Ref. 13, but only after steps were taken to eliminate secondary electron excitations. At low electron beam energies, secondary excitation processes due to backscattered electrons from the Faraday cup were appreciable and contributed as much as 13 percent to the observed intensity at 4 keV but were negligible near 20 keV. The 30-v negatively biased grid on the Faraday was more than sufficient to suppress these secondary electrons.

The theoretical calculation of the $N_2^+(1-)(0,0)$ band profile described in Section 3.0 was in excellent agreement with the experimentally obtained profile. The ratio of the R branch peak height to the P branch peak height was 0.305 for both the theoretically and experimentally determined profiles. From this measurement and those of Ref. 5 at other temperatures, it is believed that the procedure used in this paper is accurate to within less than 0.5 percent.

The apparent cross sections of the NII $^3F°$ state produced by the dissociative excitation of $N_2$ (Fig. 23) and NO (Fig. 24) over the electron beam energy range of 4 to 20 keV and plotted against the reciprocal of the electron beam energy show, as do the Bethe plots (Figs. 25 and 26), that the transition is consistent with the Bethe-Born equation for forbidden transitions. The apparent cross section of the NII $^1D$ state produced by the dissociative excitation of $N_2$ (Figs. 27 and 28) is also consistent with the Bethe-Born approximation for a forbidden transition. The apparent cross section of the NII $^1D$ differs significantly from the Bethe-Born equation below about 8 keV as shown in Figs. 29 and 30.
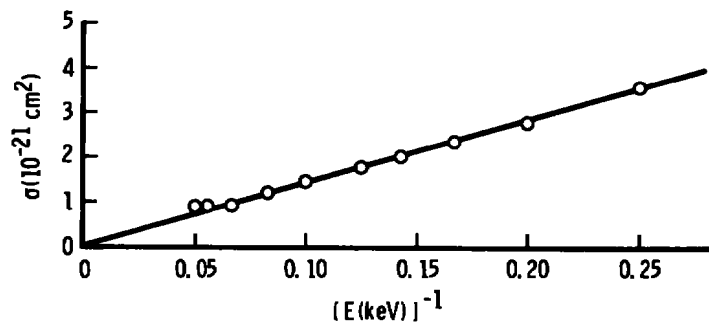
Figure 23. Energy dependence of the molecular nitrogen NII($^3$F°) apparent cross section.
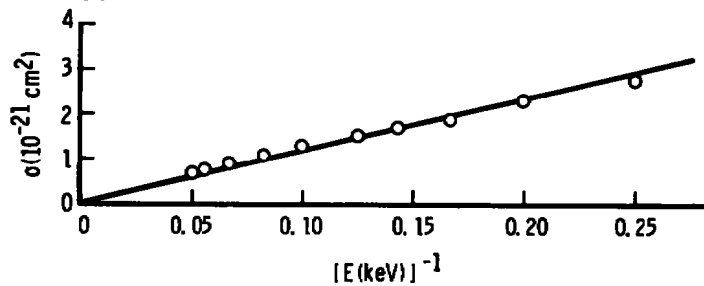


Figure 24. Energy dependence of the nitric oxide NII($^3$F°) apparent cross section.
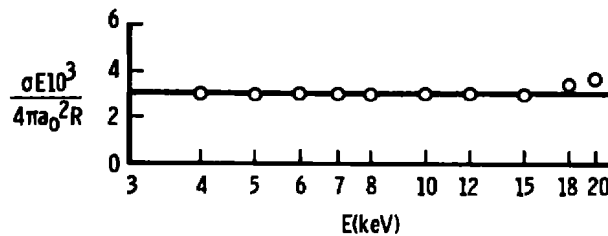


Figure 25. Bethe plot of the molecular nitrogen NII($^3$F°) apparent cross section.
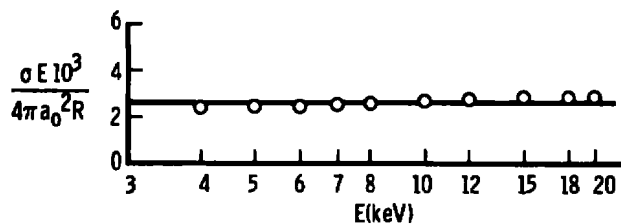


Figure 26. Bethe plot of the nitric oxide NII($^3$F°) apparent cross section.

Figure 27. Energy dependence of the molecular nitrogen NII($^1$D) apparent cross section.



Figure 28. Bethe plot of the molecular nitrogen NII($^1$D) apparent cross section.



Figure 29. Energy dependence of the nitric oxide NII($^1$D) apparent cross section.



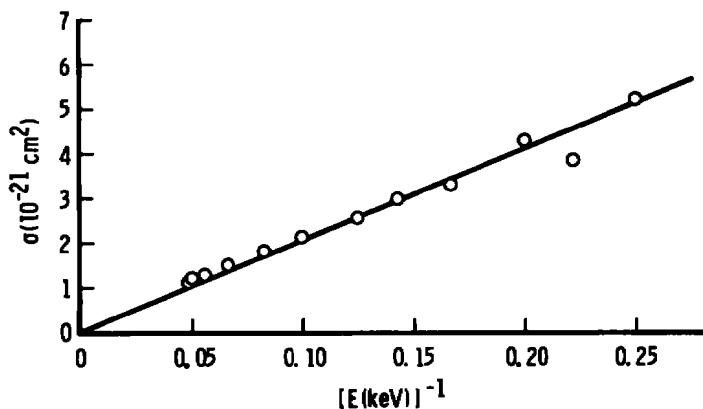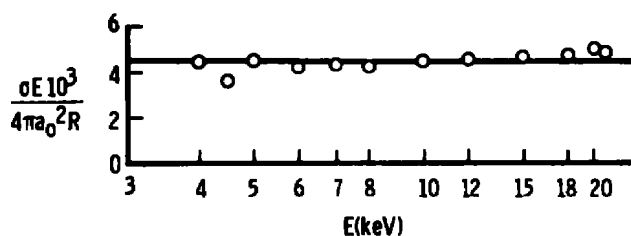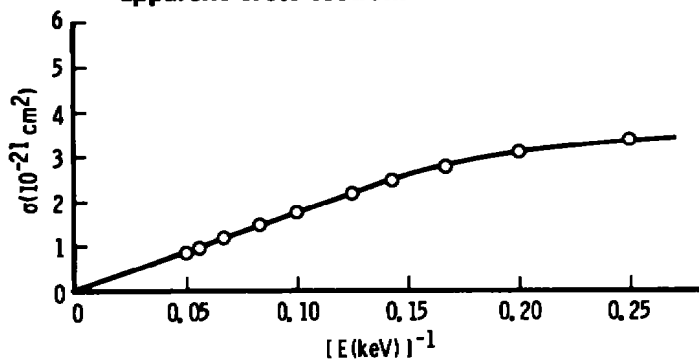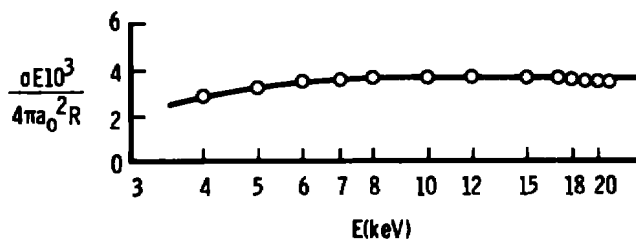Figure 30. Bethe plot of the nitric oxide NII($^1$D) apparent cross section.

The slopes as determined by the Bethe plots are $[6.1 \pm 8.3] \times 10^{-5}$, $[3.5 \pm 0.5] \times 10^{-4}$, $[2.4 \pm 2.5] \times 10^{-4}$, and $[-6.7 \pm 7.0] \times 10^{-5}$ for the $NII(N_2; 5016.4 \text{ Å})$, $NII(NO; 5016.4 \text{ Å})$, $NII(N_2; 3995.0 \text{ Å})$, and $NII(NO; 3995.0 \text{ Å})$ transitions, respectively. These values along with the respective standard deviations show a near zero or zero slope indicating that the Bethe-Born equation for a forbidden transition is applicable.

The nonlinearity below 8 keV on the $NII(NO; 3995.0 \text{ Å})$ Bethe plot (Fig. 30) may be due to the existence of two competing processes producing the same radiating $NII ^1D$ state. First, consider the possibility that the $NII ^1D$ state is produced by two competing dissociative excitation processes where one process is optically allowed and the other forbidden, the optically allowed process being dominant at the lower energies. Then as the electron beam energy is increased, the cross section of the optically allowed process becomes sufficiently small to enable the forbidden process to dominate, thus producing the observed energy dependence. Next, consider the situation where another excited state (Fig. 22) as well as the $NII ^1D$ is produced by the dissociative excitation process, the other excited state subsequently cascading into the $NII ^1D$ level. If the higher excited state is produced by an allowed process and the $NII ^1D$ state by a forbidden process, the observed behavior could result. Thirdly, it is possible that the $NII ^1D$ state is not excited by the incident electrons but is due only to two cascading transitions, one of which is produced by an allowed and the other a forbidden dissociative excitation process. Again the observe energy dependence could result. Note, however, that, in all three cases, there is one allowed and one forbidden process. For the cases where both processes are forbidden, only a different value of $b_n$ would result. Little can be said about the validity of the cascading arguments, however, as the population of these states, which may cascade with the $NII ^1D$ state, by electron collision is at present unknown.

Potential energy curves for the electronic states of $N_2$ and NO exist (Ref. 19) only for the lowest electronic levels and are not adequate to provide information regarding the excitation channels which produce $NII ^1D$ and $NII ^3F°$ excitations. In principle, however, it is well known that when a molecule in its ground electronic state undergoes a collision with a high energy electron, excited electronic states may be produced, some of which may lead to dissociation of the molecule, and the excitation processes obey the Franck-Condon principle as described in Section 1.0. Therefore, excitations may occur to stable electronic states, to electronic states from which the molecule will dissociate, and to electronic

states where both stable molecules and dissociation results. A number of electronic states of the last two types may exist and may result in the NII excitations of interest. Thus, accurate potential energy curves are needed to aid in the understanding of the physical processes involved in these excitations.

Finally, as an application of the results of this study we shall consider the use of the electron beam fluorescence technique for specie density measurements of $N_2$/He and NO/He binary mixtures. Considering the excitation of He by electron collision, it is well known that the process

$$e^- + He(1\,^1S) \rightarrow He(3\,^1P) - e^-$$
$$\quad\quad\quad\quad \lfloor\rightarrow He(2\,^1S) + h\nu(5016\,\overset{o}{A}) \quad\quad\quad (57)$$
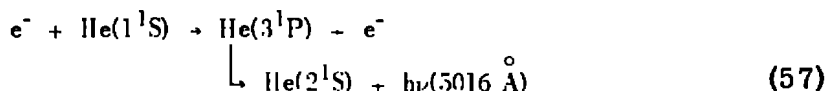
is desirable for utilization for diagnostics purposes because of the ease with which it is excited. It is recalled that both $N_2$ and NO produce radiation at 5016 $\overset{o}{A}$ from NII radiation transitions resulting from electron dissociative excitation processes. Consequently, the measured radiative intensity at 5016 $\overset{o}{A}$ observed from a binary mixture of either $N_2$/He or NO/He results from both He and either $N_2$ or NO excitations and is not a unique measure of an individual specie density. The contribution to the measured intensity by the individual species is, of course, dependent not only on the specie density but also on the individual excitation cross section. The following section will consider such mixtures and the magnitudes of the individual specie excitation cross sections for the purpose of determining binary mixture compositions for which unambiguous and accurate density measurements are possible.

Consider the interaction of an electron beam of current I and cross-sectional area (a) with a gaseous binary mixture consisting of specie 1 and specie 2 in their ground states g such that excited states i and j, respectively, are produced and a steady-state photon emission rate is observed at a wavelength $\lambda$. The volume rates of production of atoms are $(I/a)n_g^1\,\sigma_{gi}^1$ for the state i and $(I/a)n_g^2\,\sigma_{gj}^2$ for the state j, and the volume rates of radiative depopulation are given by $\sum_\ell A_{i\ell}^1\,n_i^1 = A_i^1\,n_i^1$ for the state i and $\sum_r A_{jr}^2\,n_j^2 = A_j^2 n_j^2$ for the state j, where $\sigma_{gi}^1$ is the excitation cross section of specie 1 for the g $\rightarrow$ i transition, $n_g^1$ is the specie 1 ground state number density, and $A_{i\ell}^1$ is the specie 1 Einstein transition probability for a spontaneous i $\rightarrow \ell$ transition. When it is assumed that no other processes are involved, in particular, radiative

cascading and collisional quenching effects, the steady-state number densities in states i and j are given by

$$n_i^1 = (I/a)n_g^1 \sigma_{gi}^1 / A_i^1 \qquad (58)$$

and

$$n_j^2 = (I'/a)n_g^2 \sigma_{gj}^2 / A_j^2 \qquad (59)$$

For $i \rightarrow s$ and $j \rightarrow t$ transitions, multiply each equation by the appropriate Einstein transition probability to obtain the photon emission rates per unit volume,

$$S^1 = A_{is}^1 n_i^1 = (I'/a)n_g^1 \sigma_{gi}^1 \beta_{is}^1 \qquad (60)$$

$$S^2 = A_{jt}^2 n_j^2 = (I'/a)n_g^2 \sigma_{gj}^2 \beta_{jt}^2 \qquad (61)$$

where

$$\beta_{is}^1 = A_{is}^1 / A_i^1$$

is defined as the branching factor.

The observed photon emission rate is given by

$$(S^1 + S^2)V_{observation} = (S^1 + S^2)La$$

where L is the observed electron beam length. Therefore, the observed photon emission rate S is given by

$$S = S^1 + S^2 = IL\left(n_g^1 \sigma_{gi}^1 \beta_{is}^1 + n_g^2 \sigma_{gj}^2 \beta_{jt}^2\right) \qquad (62)$$

Note that neither the photon emission rate for specie 1 nor specie 2 can be determined independently. Therefore, in a binary mixture of $N_2$/He or NO/He, for which the He mole fraction is small, the observed intensity of the He(5016 Å)$3^1P \rightarrow 2^1S$ transition, which can easily be obscured by the NII(5016.4 Å)$^1D \rightarrow {}^1P^\circ$ transition, cannot be distinguished as coming from the He or the NII transition. For the cases of $N_2$/NO, $N_2$/N, and

NO/N mixtures, Eq. (62) is changed only in that $\beta^1_{is} = \beta^2_{jt}$, and the subscripts i and j refer to the same state as do s and t. Thus, the observed intensity from an excited NII state is indistinguishable as coming from $N_2$, NO, or N.

The technique demonstrated herein applies to flow diagnostics as well as determining interesting cross section behavior. The range of mixtures of $N_2$/He and NO/He for which one can use the 5016-Å He line for flow diagnostics is determined by the relative densities, transition probabilities, and cross sections. By using the transition probabilities of Ref. 18, the optical cross section for He 5016 Å$(3^1P \rightarrow 2^1S)$ extrapolated to 10 keV from Ref. 20, and the present optical cross sections for the NII 5016.4-Å transitions, the ratios of He 5016-Å intensity to the total observed intensity at 10 keV as a function of $n_{He}/n_{N_2}$ and $n_{He}/n_{NO}$ was calculated and is shown in Fig. 31. It is seen that unless the number density of helium is several times that of $N_2$ or NO, a substantial part of the observed intensity is due to the NII transition. Thus, previous and future local specie density measurements using the He 5016-Å line must include corrections for NII 5016.4-Å contributions to the observed intensity.
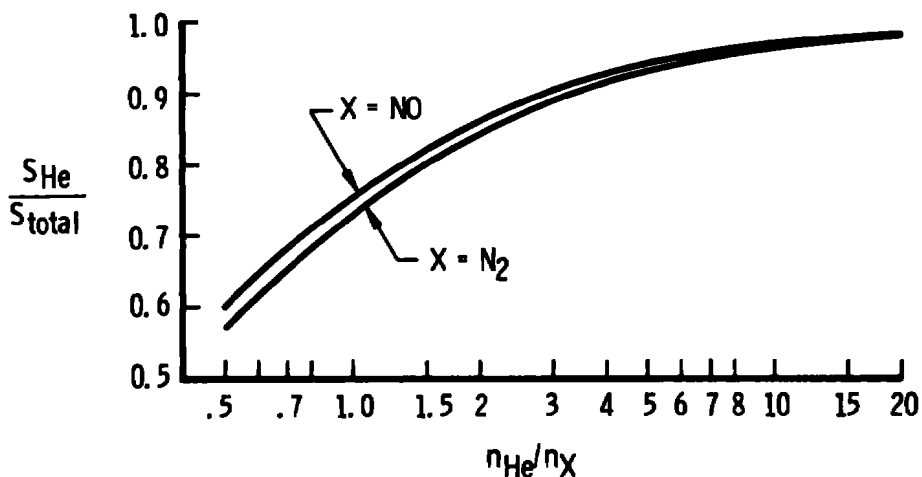


Figure 31. Ratio of helium 5016 Å to total observed intensity at 10 keV as a function of number density for $N_2$/He and NO/He mixtures.

# REFERENCES

1. Inokuti, Mitio. "Inelastic Collisions of Fast Charged Particles with Atoms and Molecules - the Bethe Theory Revisited." Rev. Mod. Phys., 43, pp. 297-347, 1971.

2. Kim, Yong-Ki and Inokuti, Mitio. "Generalized Oscillator Strengths of the Helium Atom I." Phys. Rev., 175, pp. 176-188, 1968.

3. Herzberg, G. "Molecular Spectra and Molecular Structure, I. Spectra of Diatomic Molecules." D. Van Nostrand Company, Inc., Second Edition, 1950.

4. Aarts, J. F. M. and de Heer, F. J. "Emission Cross Sections for NI and NII Multiplets and Some Molecular Bands for Electron Impact on $N_2$." Physica, 52, pp. 45-73, 1971.

5. Lewis, J. W. L., Price, L. L., and Powell, H. M. "Optical Electron Excitation Cross-Section Measurements of the $N_2^+$ First Negative System at Elevated Temperatures." AEDC-TR-73-28 (AD762257), June 1973.

6. Sharpe, J. "Dark Current in Photomultiplier Tubes." E. M. I. Electronics Ltd, Ref. No. CP. 5475, 1964.

7. Rodman, J. P. and Smith, H. J. "Tests of Photomultipliers for Astronomical Pulse-Counting Applications." Applied Optics, 2, pp. 181-186, 1963.

8. de Vos, J. C. "A New Determination of the Emissivity of Tungsten Ribbon." Physica, 20, pp. 690-714, 1954.

9. Stair, R., Johnston, R. G., and Halbach, E. W. "Standard of Spectral Radiance for the Region of 0.25 to 2.6 microns." J. Res. NBS, 64A, pp. 291-296, 1960.

10. Lewis, J. W. L., Williams, W. D., Price, L. L., and Powell, H. M. "Nitrogen Condensation in a Sonic Orifice Expansion Flow." AEDC-TR-74-36 (AD783254), July 1974.

11. Pearse, R. W. B. and Gaydon, A. G. "The Identification of Molecular Spectra." Chapman & Hall, Ltd, Second Edition, 1950.

12. Burns, D. J., Simpson, F. R., and McConkey, J. W. "Absolute Cross Sections for Electron Excitation of the Second Positive Bands of Nitrogen." J. Phys. B, 2, pp. 52-64, 1969.

13. Aarts, J. F. M., de Heer, F. J., and Vroom, D. A. "Emission Cross Sections of the First Negative Band System of $N_2$ by Electron Impact." Physica, 40, pp. 197-206, 1968.

14. Williams, W. D. "Laboratory Verification Studies of Rotational and Vibrational Temperature Measurements by the Electron Beam Technique." AEDC-TR-68-265 (AD683001), February 1969.

15. Beers, Yardley. Introduction to the Theory of Error. Addison-Wesley Publishing Co., Inc., 1957.

16. Bacon, R. H. "The 'Best' Straight Line among the Points." Am. J. Phys., 21, pp. 428-446, 1953.

17. Williams, W. D. and Lewis, J. W. L. "Rotational Temperature and Number Density Measurements of $N_2$, $O_2$, CO, and $CO_2$ in a Hypersonic Flow Field Using Laser-Raman Spectroscopy." AEDC-TR-75-37.

18. Wiese, W. L., Smith, M. W., and Glennon, B. M. "Atomic Transition Probabilities." Vol. I, NSRDS-NBS4, May 1966.

19. Gilmore, F. R. "Potential Energy Curves for $N_2$, NO, $O_2$, and Corresponding Ions." J. Quant. Spectrosc. Radiat. Transfer, 5, pp. 369-390, 1965.

20. Moustafa Moussa, H. R., de Heer, F. J., and Schutten, J. "Excitation of Helium by 0.05-6 keV Electrons and Polarization of the Resulting Radiation." Physica, 40, pp. 517-549, 1969.

## NOMENCLATURE

| | |
|---|---|
| $A_{is}$ | Einstein transition probability for spontaneous $i \to s$ transition |
| a | Electron beam cross-sectional area |
| $a_o$ | Bohr radius |
| $B^2\Sigma_u^+$ | Upper electronic state of nitrogen |
| $b_n$ | Constant defined by Eq. (33) and appearing in the excitation cross-section relation for optically forbidden transitions |
| $C_n$ | Constant defined by Eq. (30) and appearing in the excitation cross-section relation for optically allowed transitions |
| $C_1, C_2$ | Constants; $1.1909 \times 10^{-12}$ watts-cm$^2$/sr and $1.4380$ cm-K, respectively |
| c | Speed of light |
| $d\sigma_n$ | Differential cross section for excitation from ground state to state n with incident particle scattered into solid angle element $d\omega$ |
| E | Kinetic energy of incident electrons |
| $E'$ | Excitation energy |
| $E_n$ | Excitation energy from ground state to state n |
| e | Electronic charge and electron |
| $f_n$ | Optical oscillator strength |
| $f_n(K)$ | Generalized oscillator strength |
| $h\nu$ | Photon of energy $h\nu$ |
| $\hbar$ | Planck's constant divided by $2\pi$ |
| $\hbar\vec{k}$ | Initial momentum of the incident electron |
| $\hbar\vec{k}'$ | Final momentum of the incident electron |
| $\hbar\vec{K}$ | Momentum transfer of the incident electron |
| I | Electron beam current |
| $I_i$ | First ionization threshhold |
| $I_{(\lambda)}^{rel}$ | Measured relative intensity of the tungsten ribbon standard lamp using the optical system to be calibrated |

| | |
|---|---|
| $\overline{K}a_O$ | Constant defined by Eq. (28) |
| L | Observed electron beam length |
| $\tilde{M}$ | Reduced mass of the incident electron-molecule system |
| $\vec{M}$ | Vector with components $\sum\limits_{j=1}^{Z} e_j x_j$ , $\sum\limits_{j=1}^{Z} e_j y_j$ , and $\sum\limits_{j=1}^{Z} e_j z_j$ |
| $M_n^2$ | Dipole-matrix-element squared for transition from ground state to state n |
| m | Electronic mass |
| NI | Neutral atomic nitrogen |
| NII | Singly ionized atomic nitrogen |
| $N_2^+(1-)$ | First negative system of ionized molecular nitrogen |
| $N_2(2+)$ | Second positive system of molecular nitrogen |
| $N_2^+(1-)(v, v')$ | $v \rightarrow v'$ vibrational band of $N_2^+(1-)$ |
| $N_\lambda$ | Spectral radiance, watts/$cm^2$-sr-cm |
| n | Number density |
| $\hat{n}$ | Unit vector |
| $P_{nm}$ | Probability of an $n \rightarrow m$ transition |
| $\vec{p}$ | Electron momentum |
| R | Rydberg energy |
| $\vec{r}$ | Position of the incident electron relative to the center of the atom |
| $\vec{r}_j$ | Position of the atomic electrons |
| S | Photon emission rate |
| $S(\lambda)$ | Optical system relative sensitivity |
| T | True temperature |
| $T_B$ | Brightness temperature |
| V | Coulomb interaction potential energy between the incident and atomic electrons |
| $\vec{v}$ | Velocity of incident electron |
| $X^1\Sigma_g^+$ | Ground electronic state of nitrogen |

| | |
|---|---|
| $X^2\Sigma_g^+$ | Lower electronic state of nitrogen |
| $x_j$ | Component of the position vector $\vec{r}_j$ |
| $Y_{JM}$ | Spherical harmonics |
| $Z$ | Number of atomic electrons in target atom |
| $\beta_{is}$ | Branching factor for the $i \rightarrow s$ transition |
| $\epsilon(\lambda, T)$ | Emissivity |
| $\epsilon_n$ | Atomic matrix element or form factor |
| $\eta(E')$ | Efficiency or probability factor |
| $\Theta, \Phi$ | Spherical polar coordinates |
| $\theta, \phi$ | Spherical polar coordinates |
| $\lambda$ | Wavelength, $\overset{\circ}{A}$ |
| $\xi_n(\vec{r}_i, \vec{\rho})$ | Electronic wave function |
| $\rho$ | Internuclear distance |
| $\sigma_{ij}$ | Total cross section for the $i \rightarrow j$ transition |
| $\sigma_n$ | Total cross section for excitation from the ground state to state n, regardless of angle of scattering of incident particle |
| $\tau$ | Transmission factor of standard lamp quartz window |
| $\chi_{nv}$ | Vibrational wave function |
| $\Psi_{nvJM}$ | Total molecular wave function |
| $\psi_n(\vec{r}_1 \ldots, \vec{r}_z)$ | Eigenfunctions of state n and in the coordinates $\vec{r}_j$ of the atomic electrons |
| $\omega$ | Solid angle subtended by scattered electrons |